MAVEN

Mars Atmosphere and Volatile EvolutioN (MAVEN) Mission

irap
astrophysique & planétologie

Foreshock electrons impacts on hydrogen exosphere at Mars

Christian Mazelle[1], Karim Meziane[1,2], Dave L. Mitchell[3], Philippe Garnier[1], Jared R. Espley[4], Abdelhaq Hamza[2], Jasper S. Halekas[5], and Bruce M. Jakosky[6]

[1] IRAP, CNRS – University of Toulouse, UPS, CNES, France; [2] Physics Department, University of New Brunswick, Fredericton, Canada; [3] Space Sciences Laboratory, University of California, Berkeley, USA; [4] NASA Goddard Space Flight Center, Greenbelt, MD, USA; [5] Department of Physics and Astronomy, University of Iowa, Iowa City, USA; [6] LASP, University of Colorado, Boulder, USA

Planetary Atmospheric Erosion – Europlanet Workshop 2018, Romania, June 11-15, 2018

Terrestrial Foreshock

Energetic electrons and ions emanating from the bow shock (backstreaming particles)

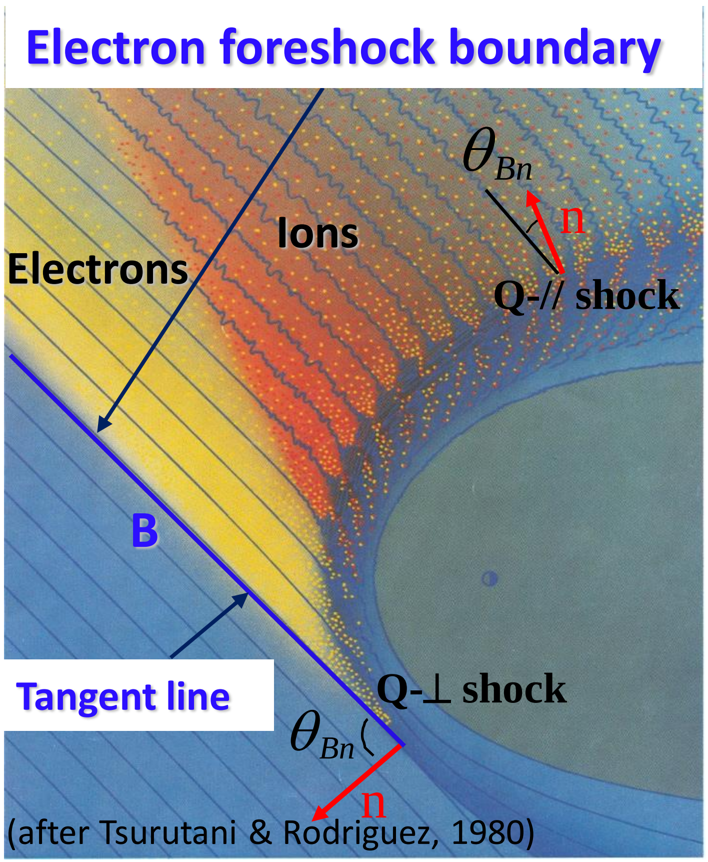

(after Tsurutani & Rodriguez, 1980)

Energetic electrons spatially organized as sheets with depths that scale with 1/v// (electron parallel velocity).
Electrons energy between 10 eV to ~100 keV.
Mostly energetic observed close to θ_{Bn} = 90°
i.e. close to the tangent line (Anderson et al., JGR, 1979)

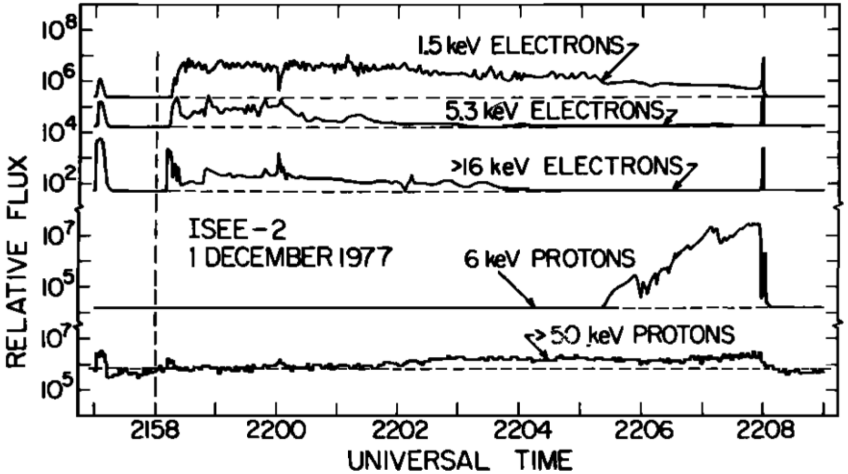

Fluxes highest near the perpendicular shock and then drop very quickly toward the quasi-parallel region.

Velocity filtering due to the solar wind electric field convection makes the foreshock electrons and ions appear spatially separated.

Mars *vs.* Earth

	Non magnetized	Magnetized
• Planet	R	1.87×R
• Solar Wind	V	V
• IMF	B	2.5×B
Parker spiral	57°	45°
• Bow shock	a_S/b_S	327×(a_S/b_S)

parabolic fit: $X = a_s - b_s\sqrt{Y^2 + Z^2}$

- Electron energization resulting from a drift along the shock gives a ratio for $\theta_{Bn} = 90°$ (maximum acceleration):

$$q_{90} \sim \frac{B_E}{B_M}\frac{\sin\phi_E}{\sin\phi_M}\frac{b_{sM}}{b_{sE}} \sim 60$$

$\phi : cone\ angle$

Earth: Emax ~100 keV

⇒ < ~2 keV for Mars

Within the range of MAVEN electron spectrometer

(3 eV – 4.6 keV)

MAVEN Mission Architecture

Launch on 18 Nov 2013
Orbit Insertion on 21 Sept 2014

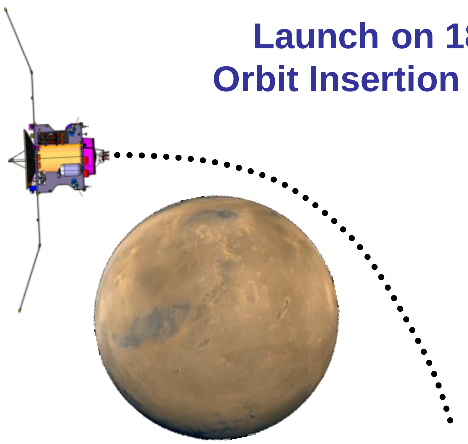

> Three Years of Science Operations

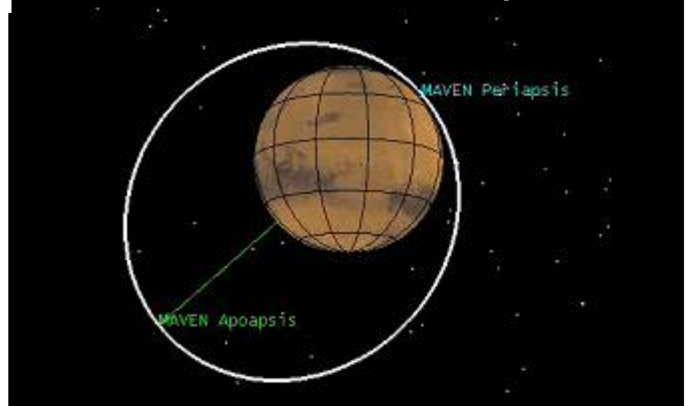

Orbit shown to scale

Orbit Precession Provides Coverage

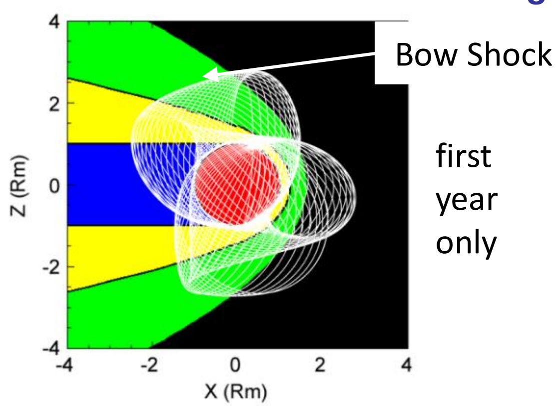

Deep Dips Cover All Altitudes

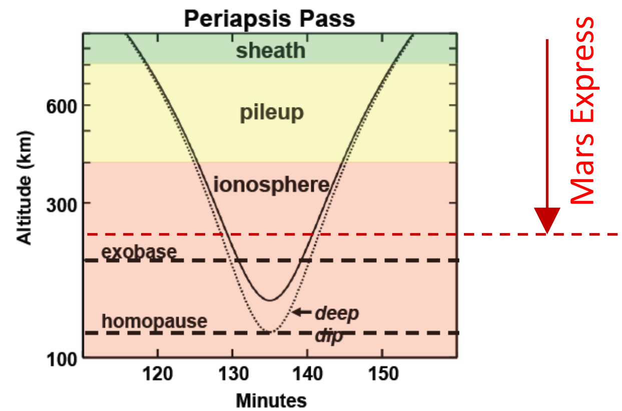

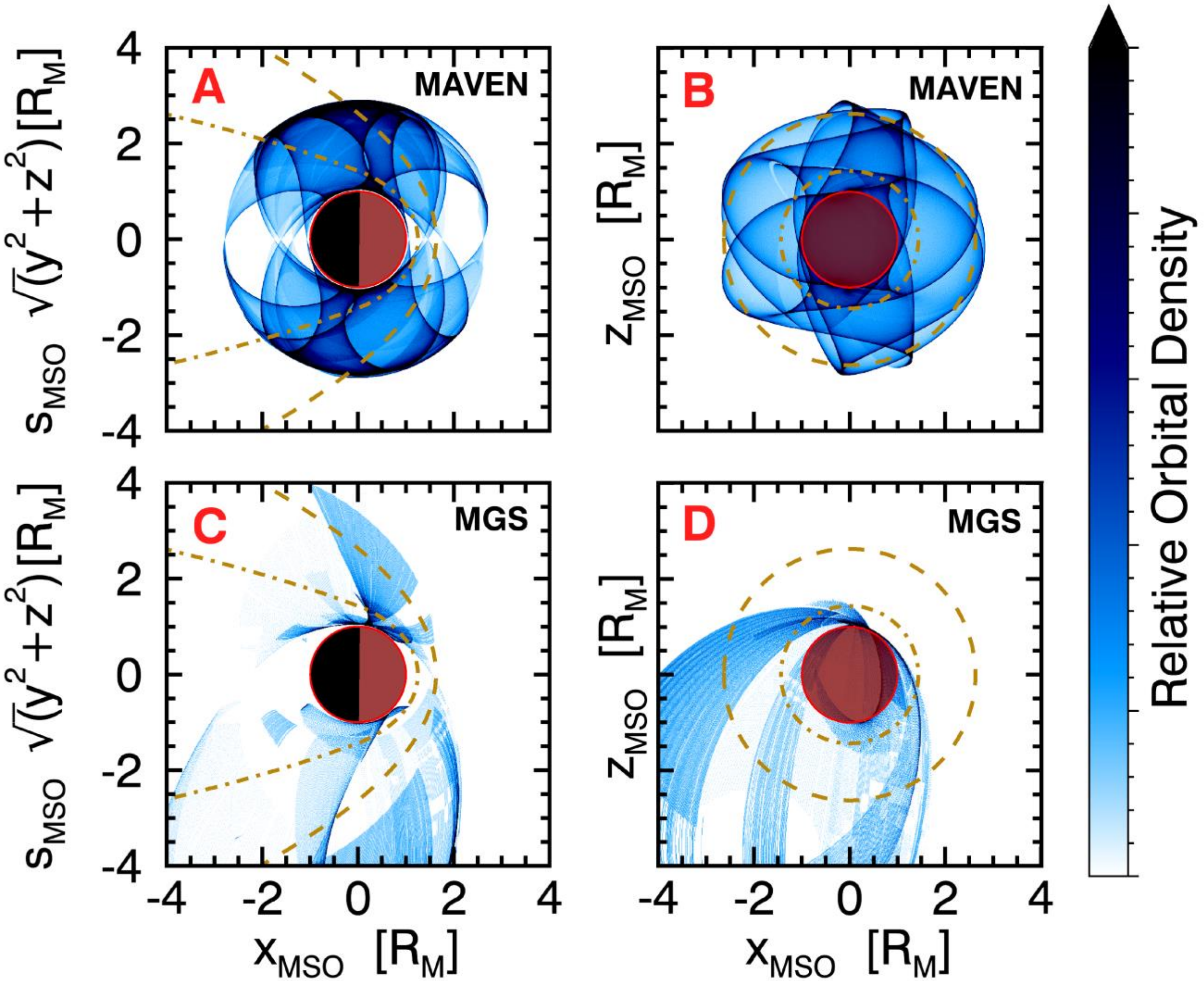
A
MAVEN
B
MAVEN
C
MGS
D
MGS
s_{MSO} $\sqrt{(y^2+z^2)}$ [R_M]
z_{MSO} [R_M]
x_{MSO} [R_M]
Relative Orbital Density

The MAVEN Science Instruments

Mass Spectrometry Instrument

NGIMS

Neutral Gas and Ion Mass Spectrometer; Paul Mahaffy, GSFC
Mehdi Benna

Particles and Fields Package

STATIC

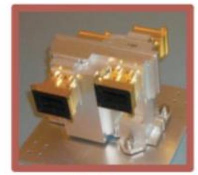

SEP

SupraThermal And Thermal Ion Composition; Jim McFadden, SSL

Solar Energetic Particles; Davin Larson, SSL

Remote-Sensing Package

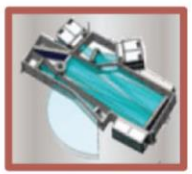

IUVS

Imaging Ultraviolet Spectrometer; Nick Schneider, LASP

SWEA

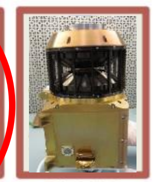

SWIA

Solar Wind Electron Analyzer; David Mitchell, SSL
Christian Mazelle, IRAP

Solar Wind Ion Analyzer; Jasper Halekas, SSL

Radio-Occultation Science Experiment

Paul Whithers, LASP

LPW

MAG

Langmuir Probe and Waves - EUV; Bob Ergun, **Laila Andersson, LASP**

Magnetometer; Jack Connerney, **Jared Espley, GSFC**

The MAVEN instruments form a comprehensive set and all closely based on similar instruments that have flown on previous missions.

The Martian Electron Foreshock

Example of case study

02/Jan/2015

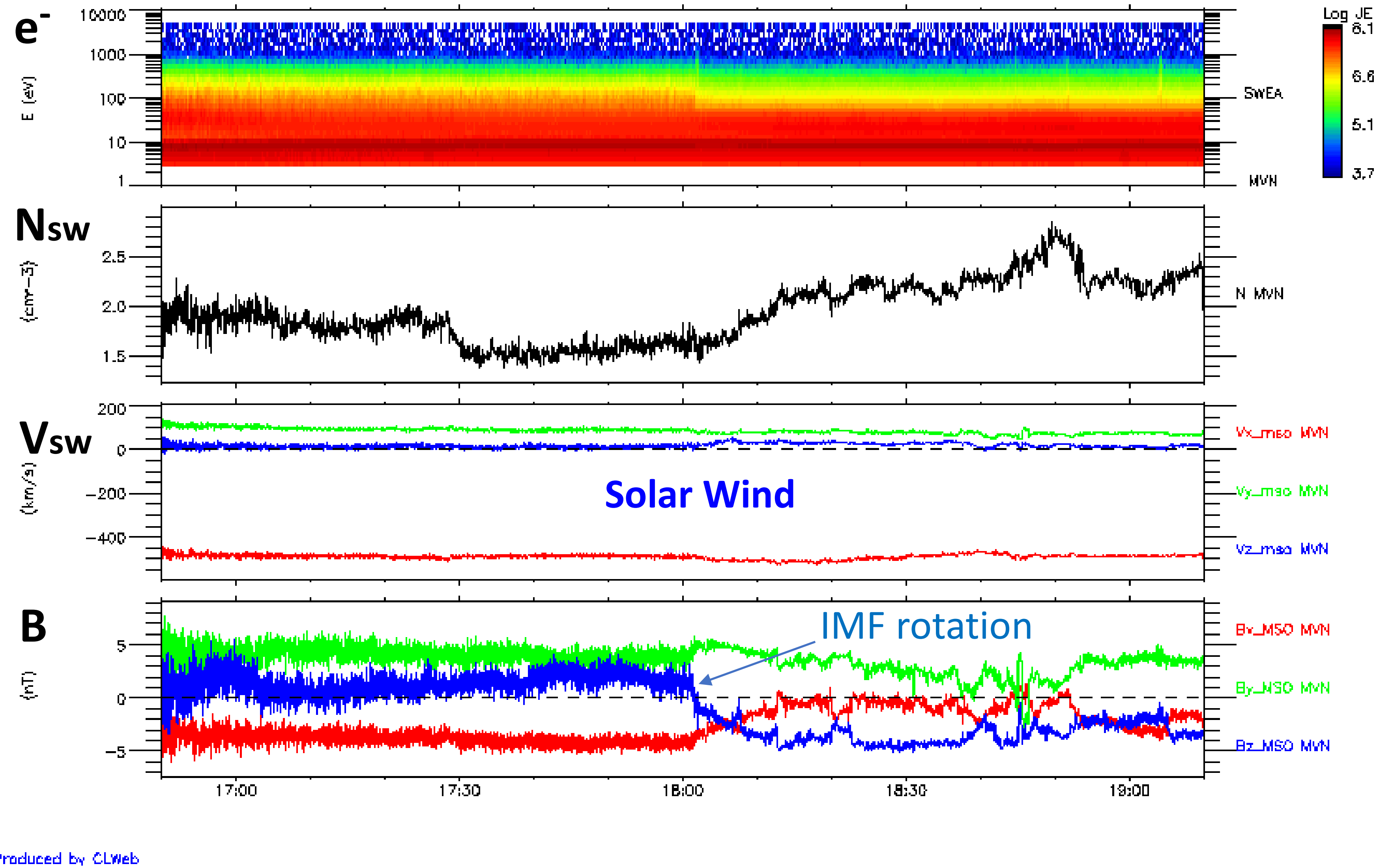

The Martian Electron Foreshock

Example of case study

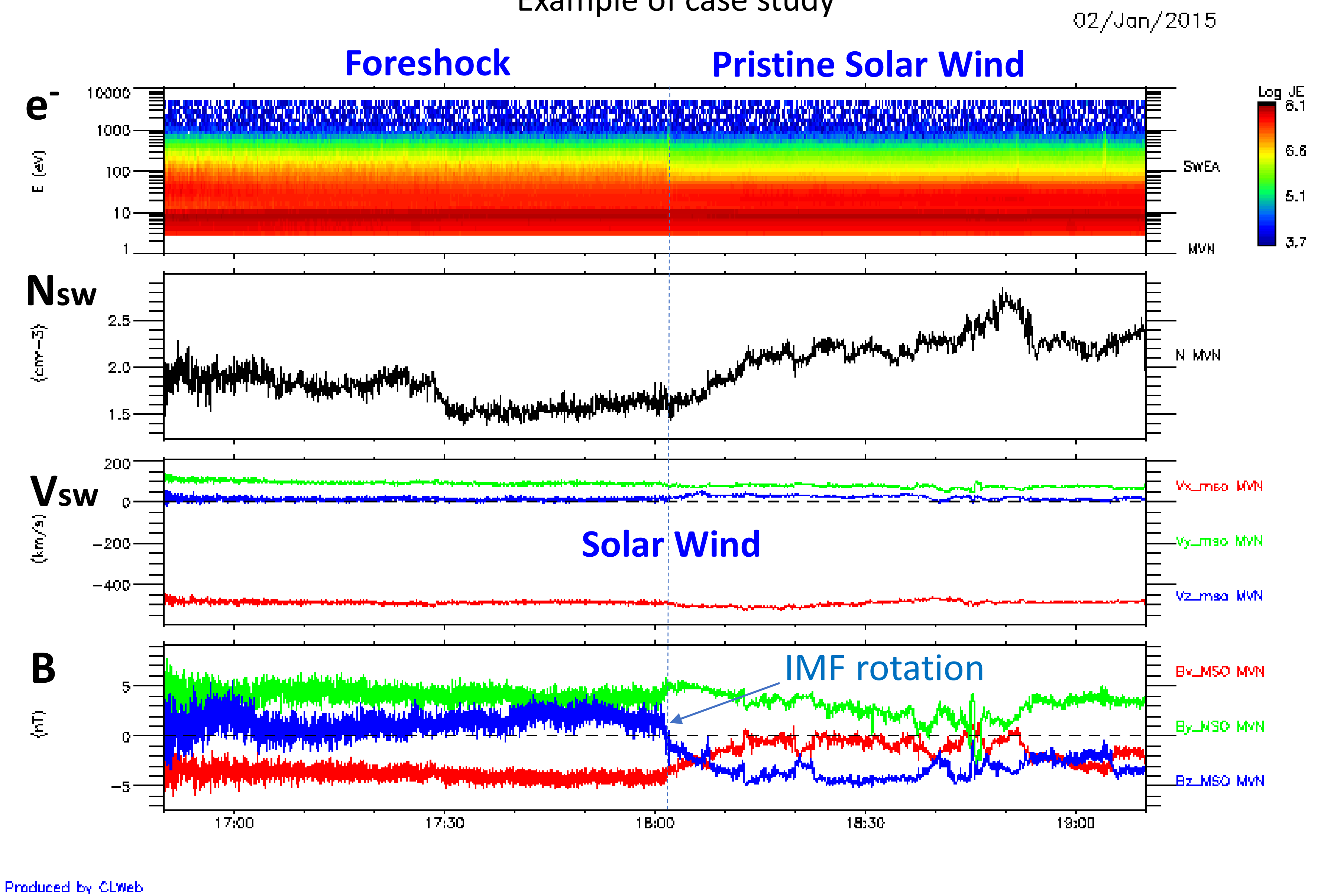

The Martian Electron Foreshock

Example of case study

02/Jan/2015

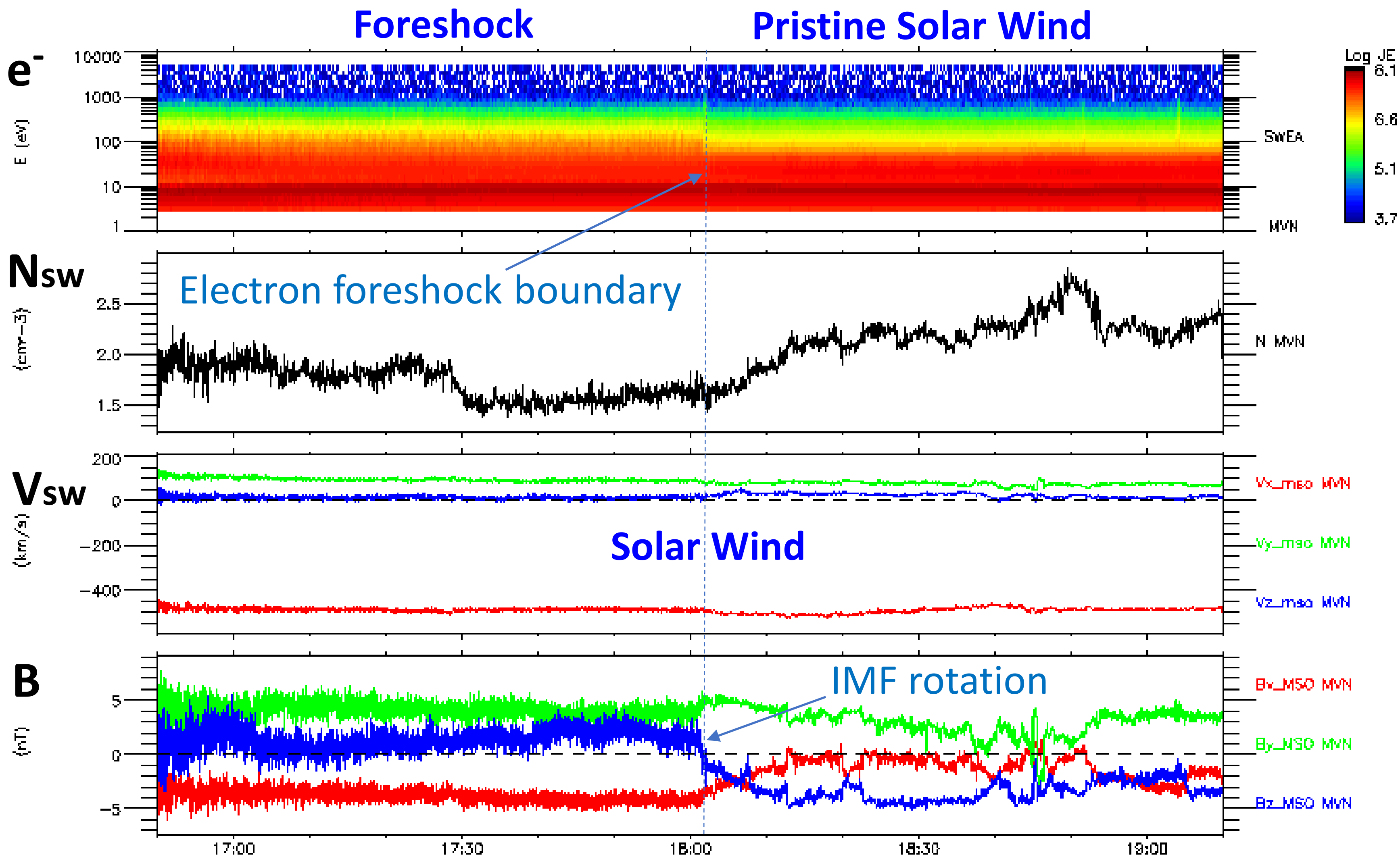

Produced by CLWeb

Geometry of the observations

Example of one case study

Maven 2015 January 02, 1650 - 1915 UT

Meziane et al., *JGR SP*, 2017

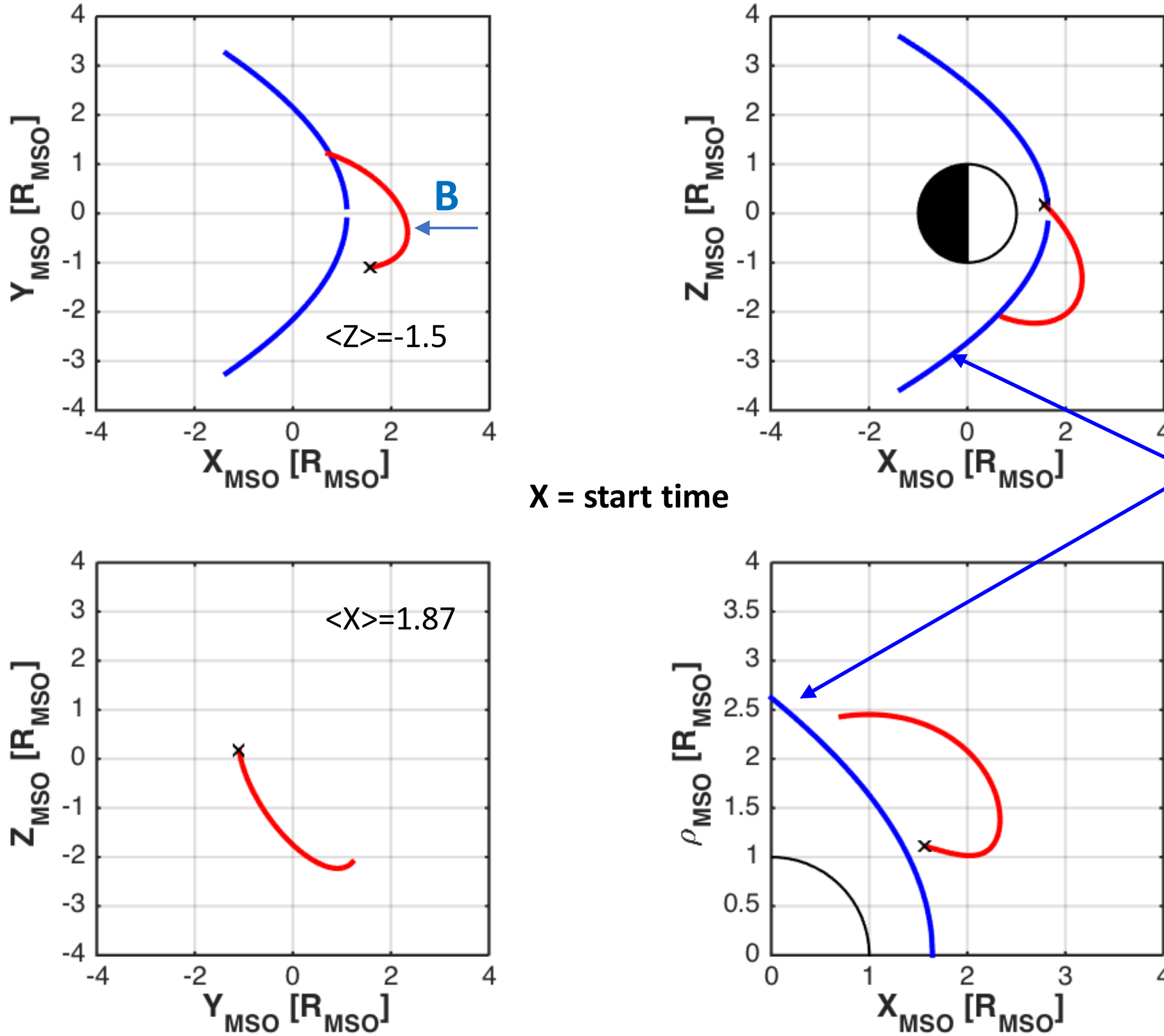

Mostly Radial IMF

Bow shock model
Vignes *et al.*, 2000
(from MGS data)

s/c going away
from the shock
first and then
coming back

Foreshock Geometry

3 major geometrical parameters:

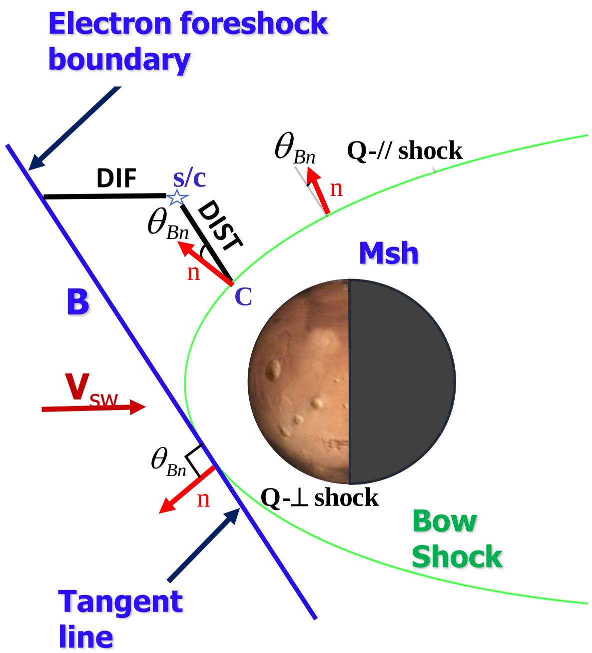

1. θ_{Bn} : Angle between the interplanetary magnetic field line and the shock normal at the connection point (model).

2. **DIST** : distance between the s/c and the shock connection point along a straight line parallel to the IMF average.

3. **DIF** : distance of the s/c from the **tangent** field line along the X_MSO axis (Mars–Sun line)

Depth inside the foreshock (negative if no connection)

Foreshock Geometry

3 major geometrical parameters:

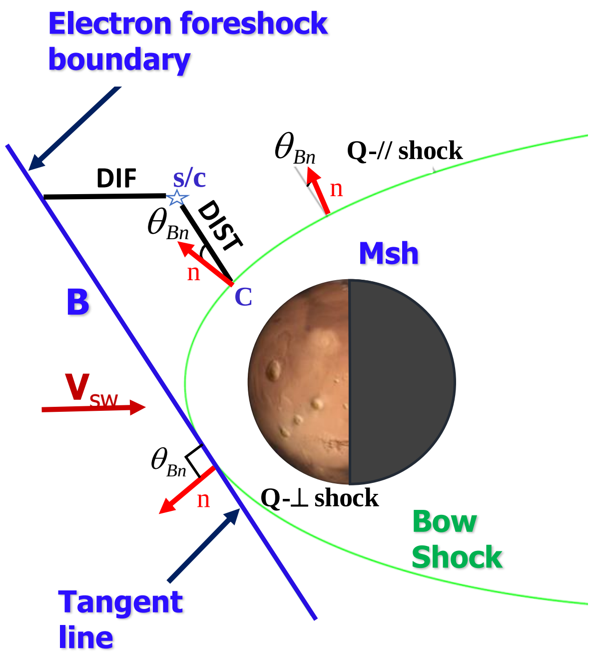

1. θ_{Bn} : Angle between the interplanetary magnetic field line and the shock normal at the connection point (model).

2. **DIST** : distance between the s/c and the shock connection point along a straight line parallel to the IMF average.

3. **DIF** : distance of the s/c from the **tangent** field line along the X_MSO axis (Mars–Sun line)
Depth inside the foreshock (negative if no connection)

Use of a bow shock model [Vignes *et al.*, 2000]
Conic section (axisymetric) from a fit of bow shock crossing locations by Mars Global Surveyor.

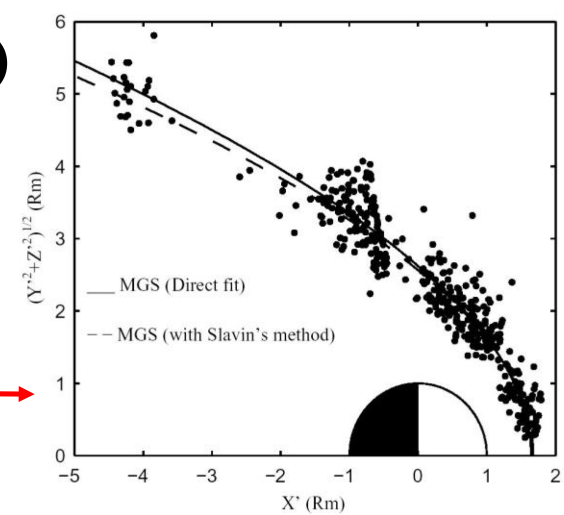

First Martian electron foreshock study at Mars by MAVEN

Meziane et al., *JGR*, 2017

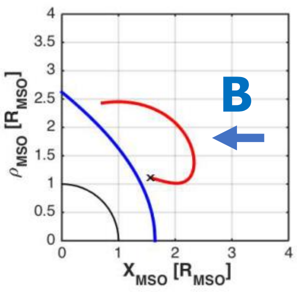

Mostly Radial IMF towards the planet

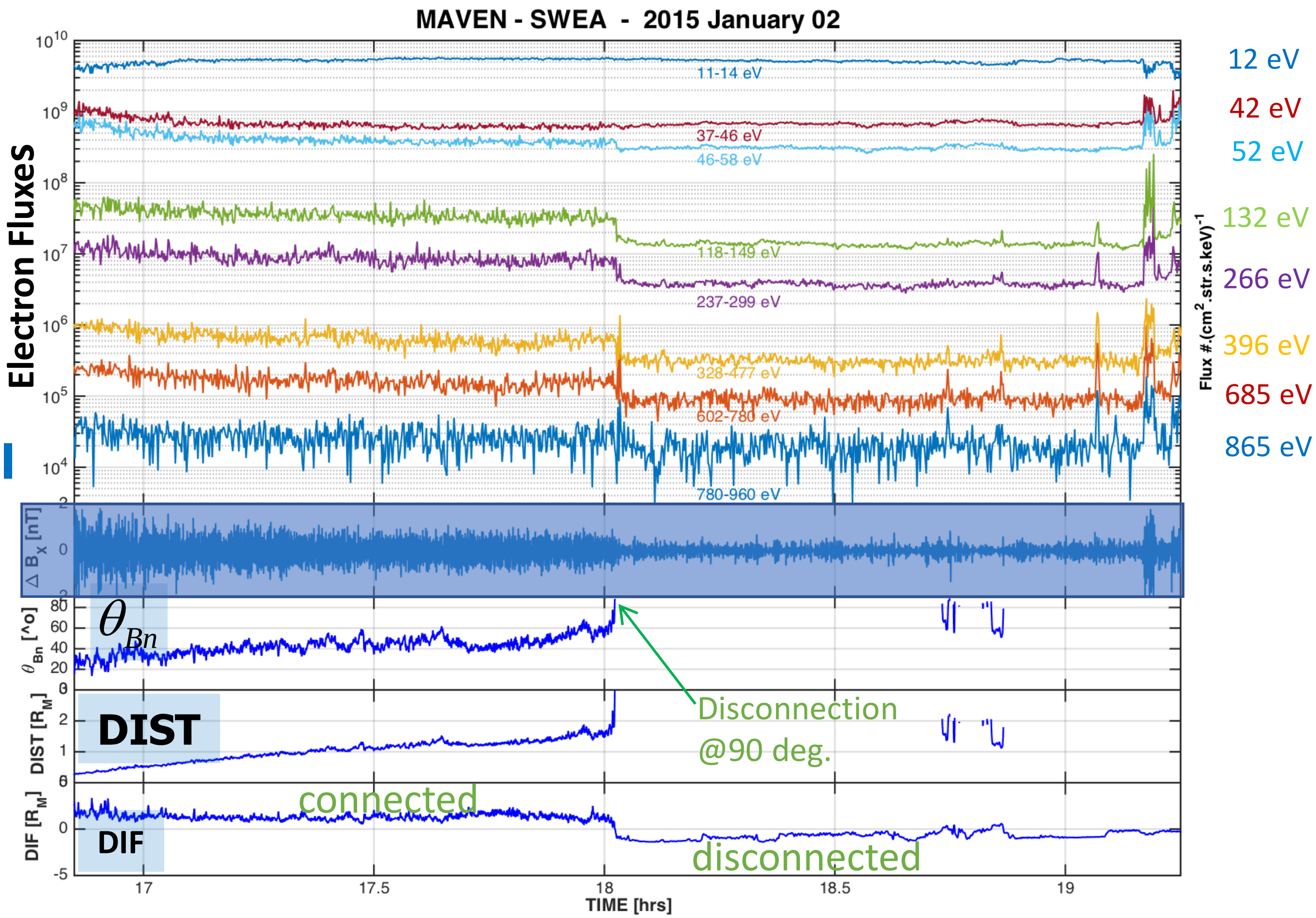

Observations vs connection model

Meziane et al., *JGR*, 2017

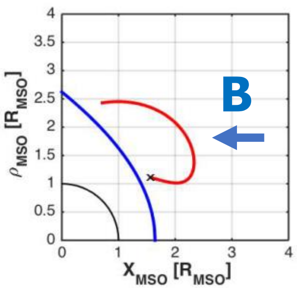

Mostly Radial IMF towards the planet

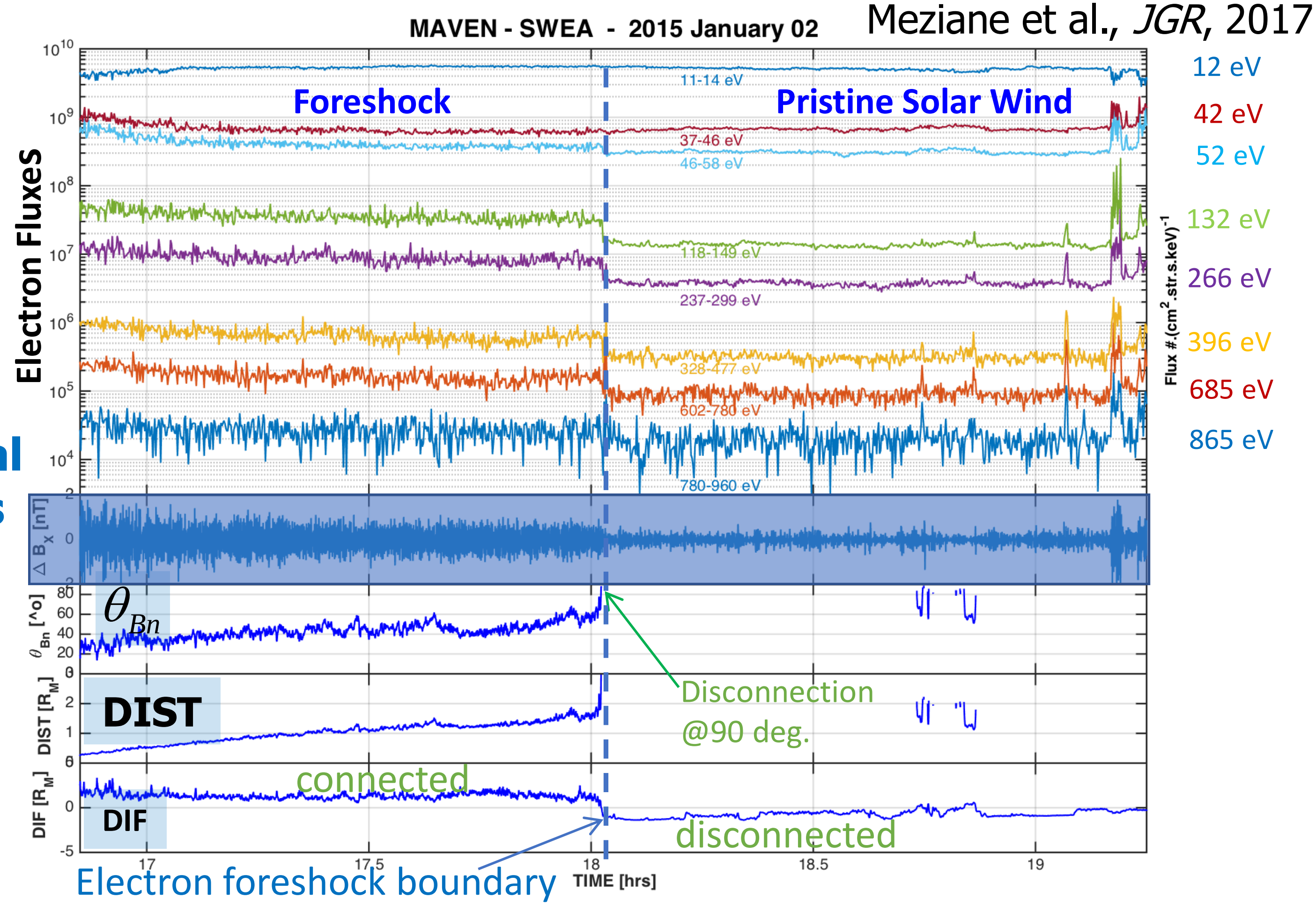

Adiabatic shock reflection (1)

[Leroy & Mangeney, 1984; Wu, 1984] **Fast Fermi Acceleration**

In the case of an adiabatic magnetic mirror reflection of a particle off the shock, the reflected particle gets a parallel velocity $v_{//r} = -v_{//i}$ **in dHT frame of reference** while the perpendicular velocity $v_\perp$ remains unchanged ('elastic encounter'):

$$\mathbf{V}_{dHT} = \mathbf{n}\times(\mathbf{V}_{SW}\times\mathbf{B}_1)/\mathbf{B}_1\cdot\mathbf{n}$$

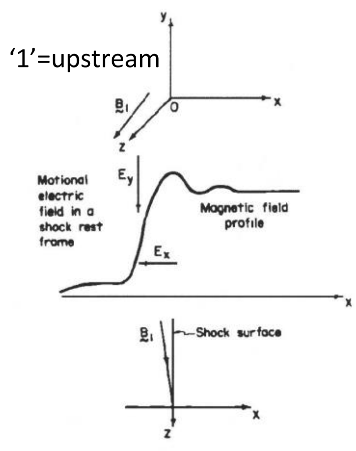

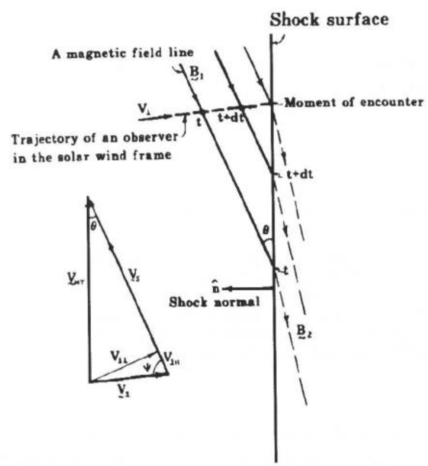

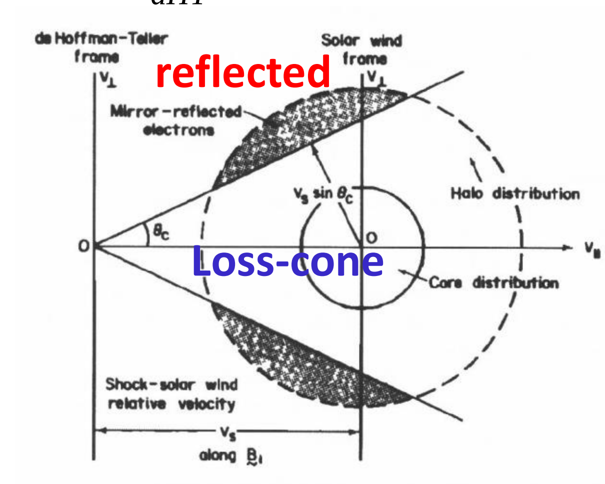

In the plasma rest frame, the particle gets a parallel velocity $v_{//r} = -v_{//i} + 2V_S$

where V_S is the shock speed such as $\mathbf{V}_S = \mathbf{V}_{SW} - \mathbf{V}_{dHT}$

or $V_S = V_{SW} \times \cos\theta_{Vn} / \cos\theta_{Bn}$ → **For large θ_{Bn} the particle can gain a large energy**

Adiabatic shock reflection and Fast Fermi Acceleration

[Leroy & Mangeney, 1984; Wu, 1984]

In the case of an **adiabatic magnetic mirror reflection** of a particle off the shock, the reflected distribution is peaked at a pitch-angle α_C **in dHT frame of reference if NO cross shock potential :**

(no motional Electric field: energy conserved)

$$cos\alpha_C = \sqrt{1 - \frac{1}{N}}$$

where $N = B_2/B_1 = B_{down}/B_{ups}$ shock compression ratio

In the plasma rest frame of reference if NO cross shock potential $\Delta\Phi = 0$:

$$cos\alpha_C = \left(\frac{1}{N}\right)\left(\eta + \sqrt{(N-1)(N-\eta^2)}\right)$$ [Decker, 1983]

where $\eta^2 = E_S/E$ (<1) **Energy-dependent**

E = particle energy (in the plasma rest frame)

E_S (energy corresponding to shock speed or **dHT** velocity with respect to the plasma frame):

$$\mathbf{V}_S = \mathbf{V}_{SW} - \mathbf{V}_{dHT} \qquad V_S = V_{SW} \times \cos\theta_{Vn} / \cos\theta_{Bn}$$

In the plasma rest frame, the particle gets a parallel velocity:

$$v_{//r} = -v_{//i} + 2V_S$$

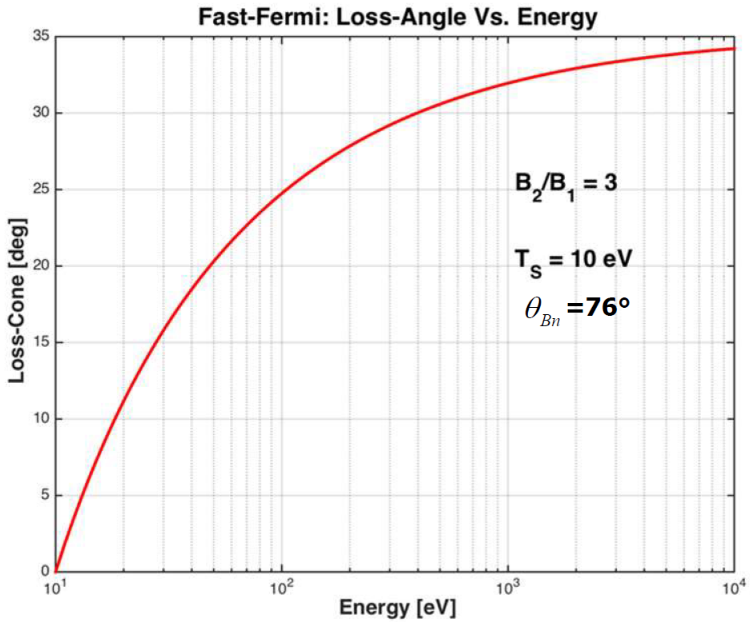

For large θ_{Bn} the particle can gain a large 'boost' in energy from a single reflection (Fast Fermi)

Observations

Meziane et al., *JGR*, 2017

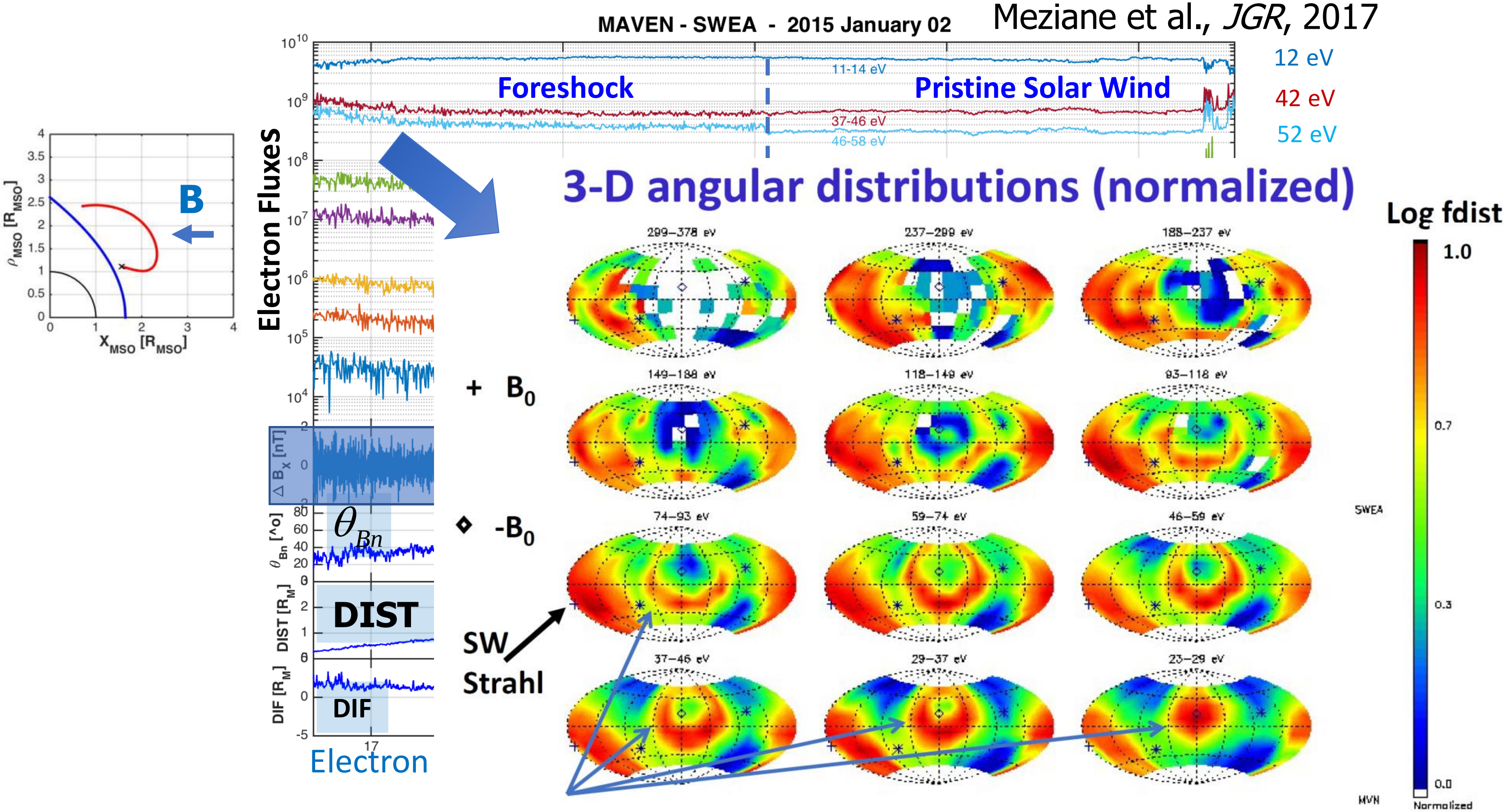

B_0 towards Mars

Annulus (ring-beam) around $-B_0$ with an energy-dependent radius (increasing with energy) moving sunward ⟶ backstreaming electrons

Observations

Pitch-Angle Distributions

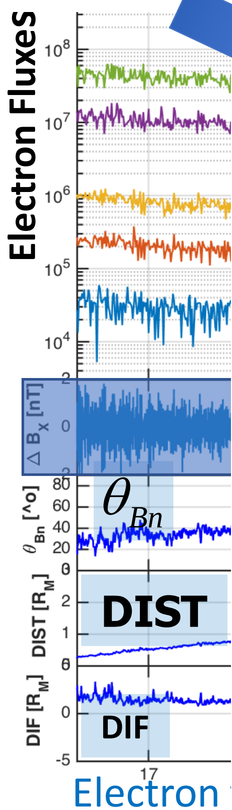

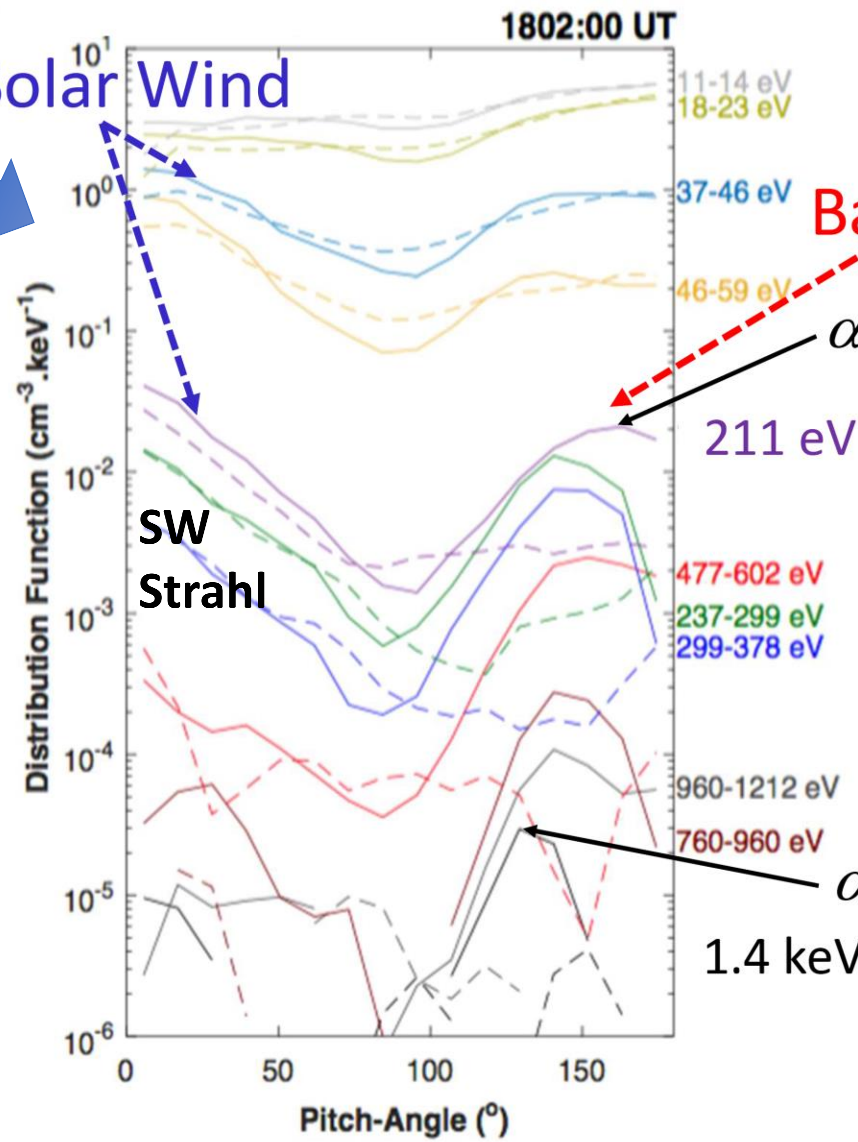

Peak pitch-angle (ring-beam) decreases with energy: larger loss cone.

Observations vs connection model

Pitch-Angle Distributions

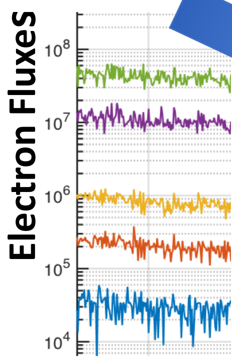

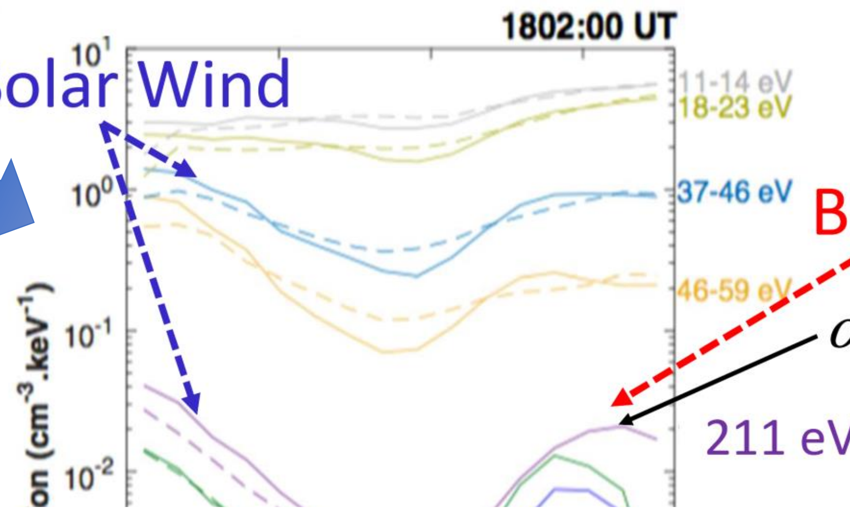

Peak pitch-angle (ring-beam) decreases with energy: larger loss cone.

These characteristics are consistent with magnetic mirror adiabatic reflection at the bow shock: Fast Fermi acceleration [Wu, 1984; Leroy & Mangeney, 1984].

$\alpha \approx 130°$

Electron

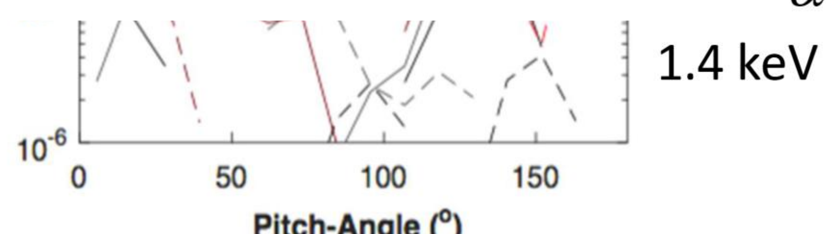

Adiabatic shock reflection: role of cross-shock potential

Loss cone angle **with cross-shock potential**
(all the physical quantities are in plasma rest frame):

$$cos\alpha_c = \frac{1}{N}\left[\eta + \sqrt{(N-1)(N-\eta^2) - N\eta^2(e\Phi_S/E_S)}\right]$$

with $N = \frac{B_2}{B_1}$ and $\eta^2 = \frac{E_S}{E}$

The inflection point occurs for the energy such that:

$$\frac{dcos\alpha_c}{d\eta} = 0 \rightarrow \eta^2 = \frac{1}{2}\frac{N(N-1)}{(N-1) + N(e\Phi_S/E_S)}$$

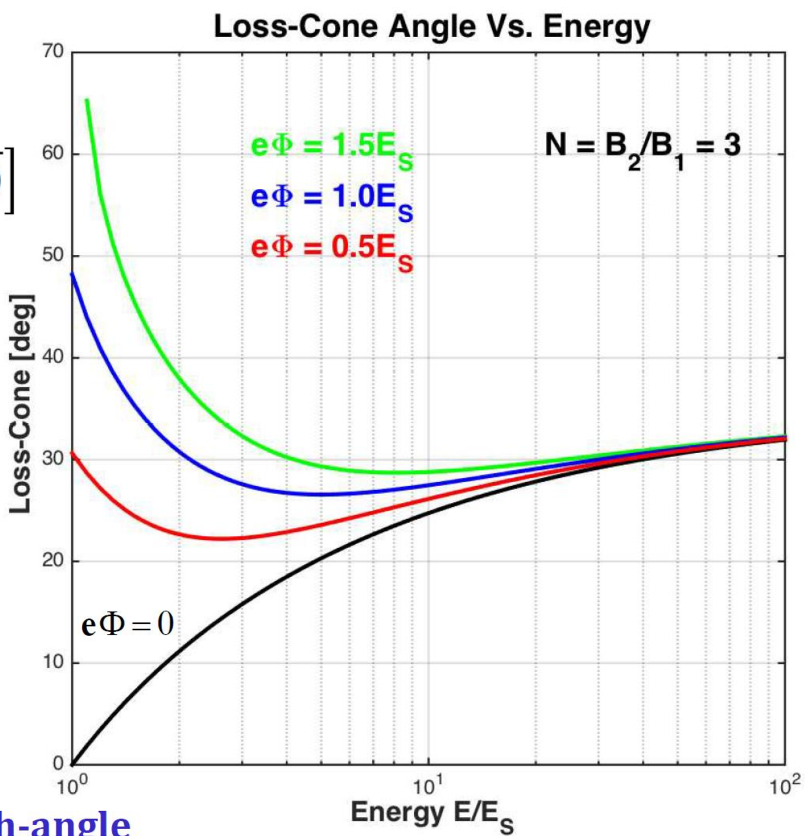

The variation of the Foreshock electrons PEAK pitch-angle versus their energy can be used to remotely constraint the cross-shock potential

3-D angular distributions

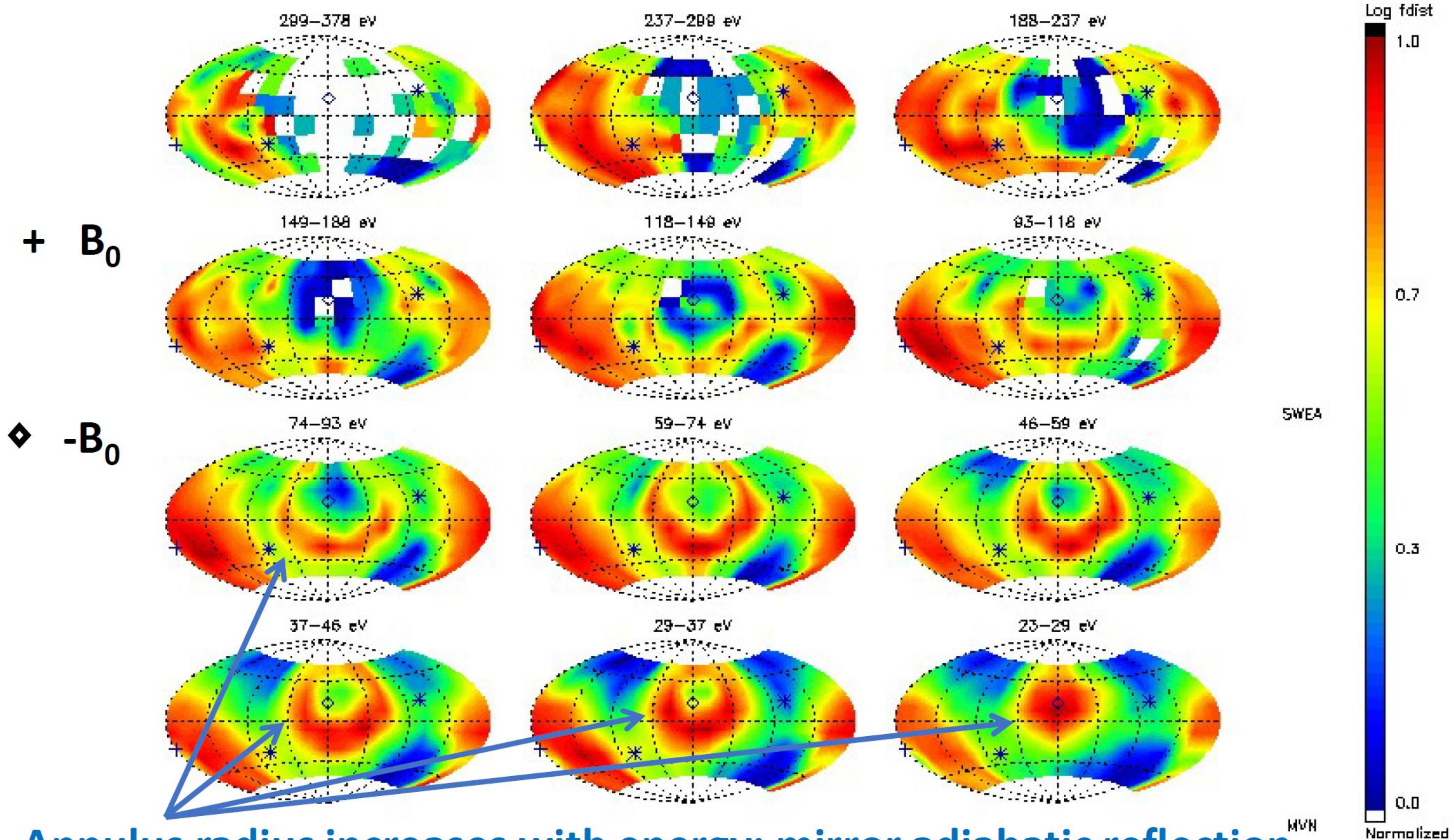

Annulus radius increases with energy: mirror adiabatic reflection with very small cross-shock potential

Produced by CLWeb

Production mechanism
Adiabatic shock reflection: computation of reflected fluxes

Solar wind electrons reflect off the shock in an adiabatic manner (conservation of magnetic moment). The pre (post) shock-encounter particle energy E_i (E) and pitch angle $\mu_i = \cos\alpha_i$ ($\mu = \cos\alpha$) in the plasma frame of reference are given by:

$$\frac{E_i}{E} = 1 + 4 \times \frac{E_S}{E} - 4 \times \mu \times \sqrt{\frac{E_S}{E}} \qquad \mu_i = \frac{\mu - \sqrt{\frac{E_S}{E}}}{\sqrt{\frac{E_i}{E}}}$$

E_S = Energy corresponding to the shock speed V_s :

$$\mathbf{V}_S = \mathbf{V}_{SW} - \mathbf{V}_{dHT} \qquad V_S = V_{SW} \times \cos\theta_{Vn} / \cos\theta_{Bn}$$

Conservation of phase-space density along the orbit (**Liouville's theorem**): Reflected distribution

$$f_r(E,\mu) = f_{SW}(E_i(E,\mu), \mu_i(E,\mu))$$

f_{SW} : seed population obtained by fitting with a kappa distribution of a pristine solar wind distribution.

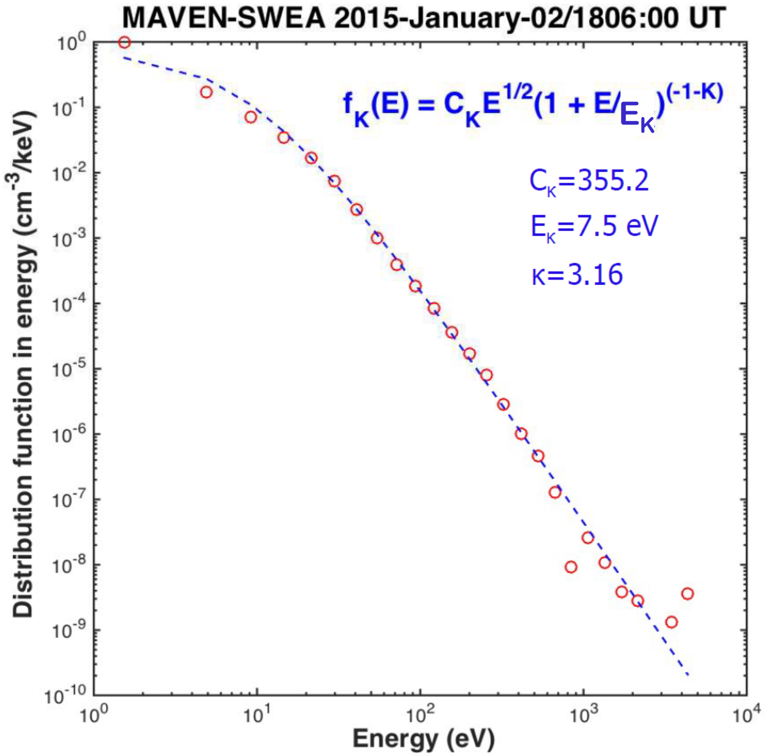

Production mechanism
Adiabatic shock reflection: computation of reflected fluxes

Solar wind electrons reflect off the shock in an adiabatic manner (conservation of magnetic moment). The pre (post) shock-encounter particle energy E_i (E) and pitch angle $\mu_i = \cos\alpha_i$ ($\mu = \cos\alpha$) in the plasma frame of reference are given by:

$$\frac{E_i}{E} = 1 + 4 \times \frac{E_S}{E} - 4 \times \mu \times \sqrt{\frac{E_S}{E}} \qquad \mu_i = \frac{\mu - \sqrt{\frac{E_S}{E}}}{\sqrt{\frac{E_i}{E}}}$$

E_S = Energy corresponding to the shock speed V_s :

$$\mathbf{V}_S = \mathbf{V}_{SW} - \mathbf{V}_{dHT} \qquad V_S = V_{SW} \times \cos\theta_{Vn} / \cos\theta_{Bn}$$

Conservation of phase-space density along the orbit (**Liouville's theorem**): Reflected distribution

$$f_r(E,\mu) = f_{SW}(E_i(E,\mu), \mu_i(E,\mu))$$

f_{SW} : seed population obtained by fitting with a kappa distribution of a pristine solar wind distribution.

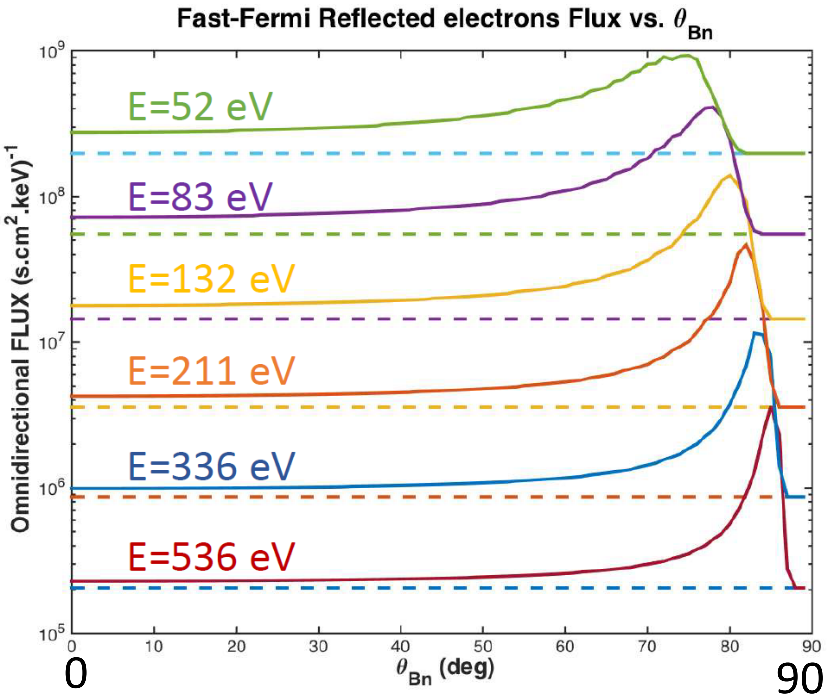

0 90

Fluxes increase with θ_{Bn}

Puzzling observations

(1)

Flux fall-off above ~30 eV when θ_{Bn} increases !

Meziane et al., *JGR*, 2017

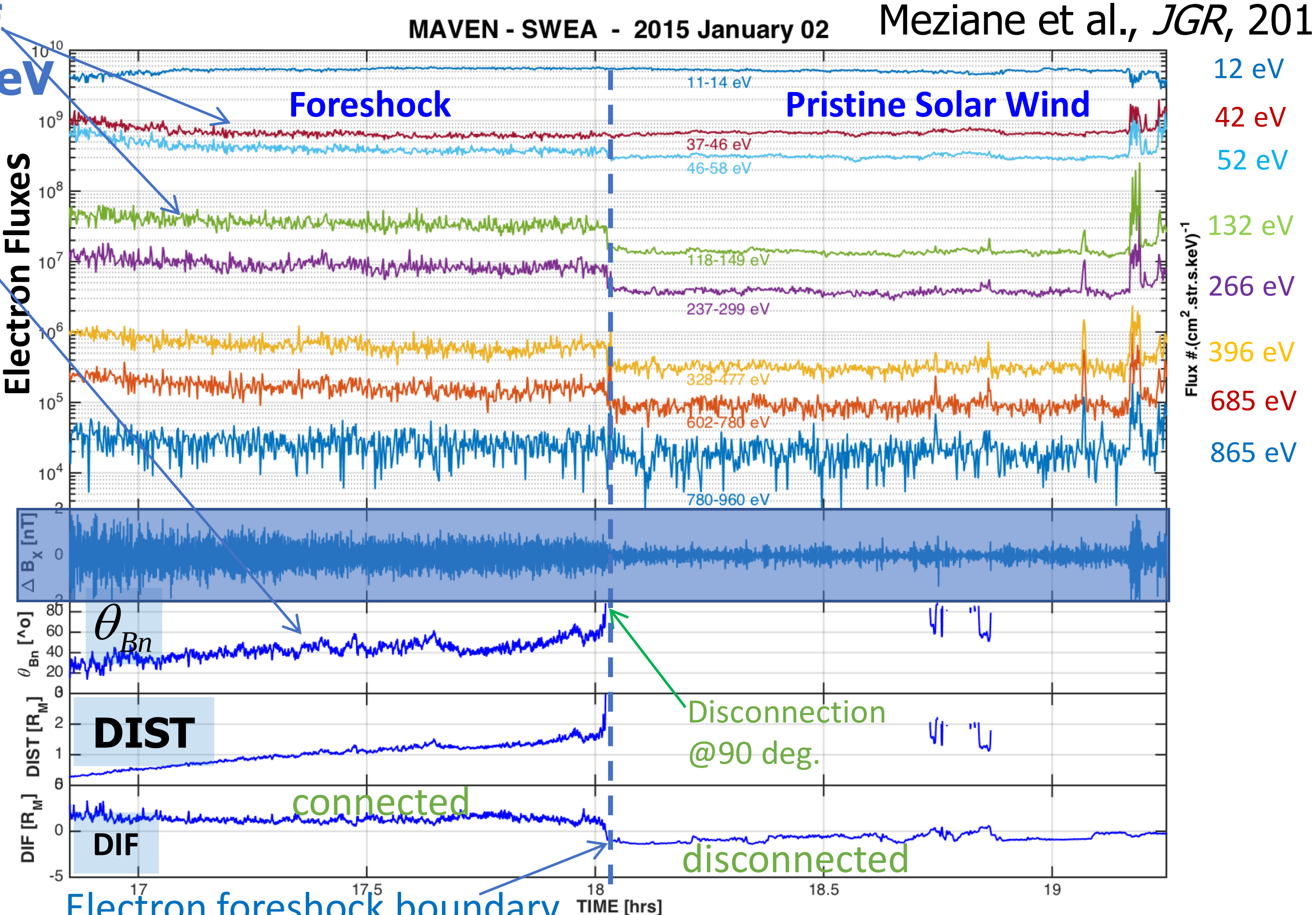

Apparent discrepancy with the theory for the variation versus θ_{Bn} !... Why?

Puzzling observations

(1)

Flux fall-off above ~30 eV when θ_{Bn} increases ! but also DIST

Meziane et al., *JGR*, 2017

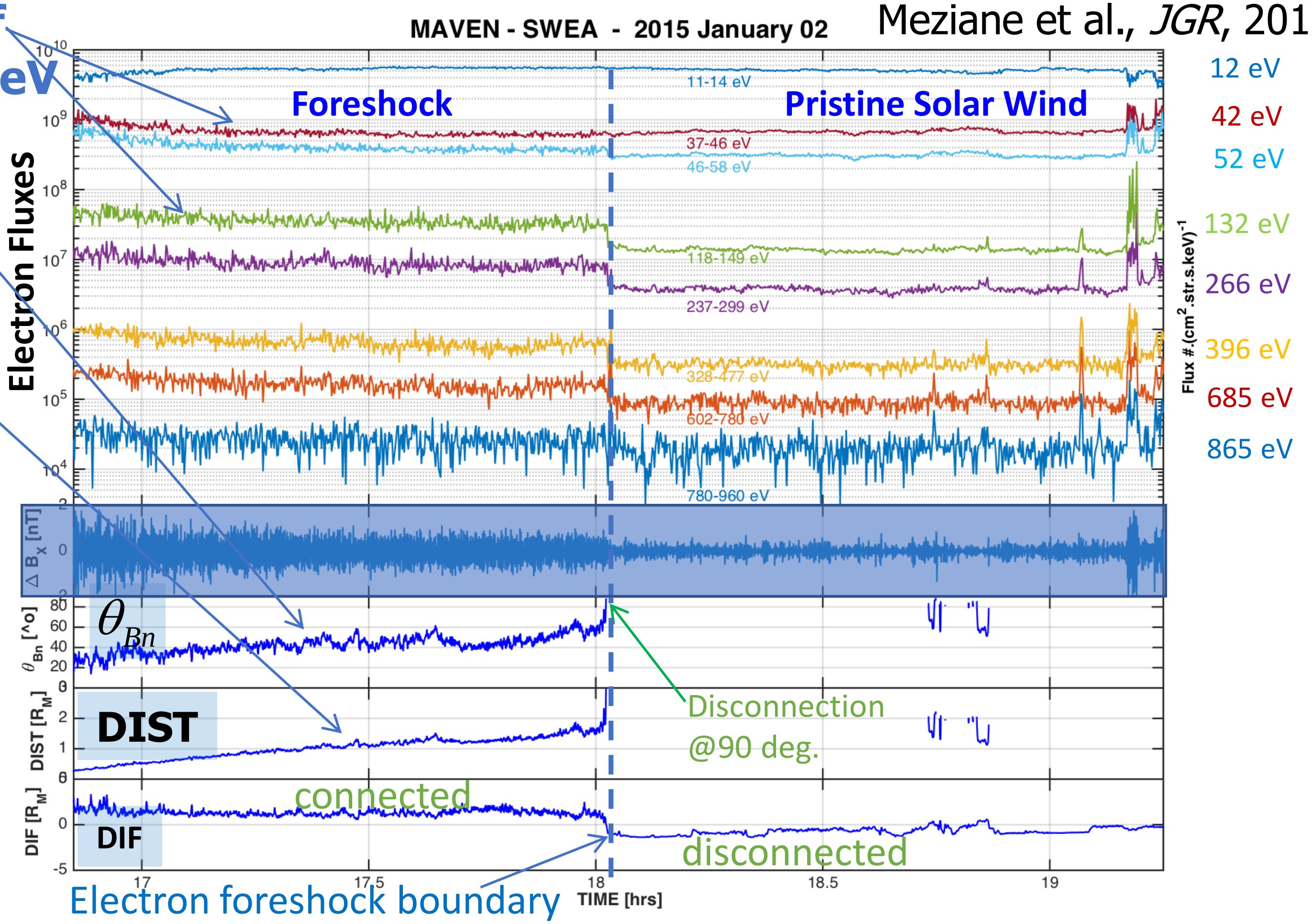

Apparent discrepancy with the theory for the variation versus θ_{Bn} !… Why?

The distance along the magnetic field is more relevant for the flux decay.

Puzzling observations

(1)
Flux fall-off above ~30 eV when θ_{Bn} increases ! but also DIST

Meziane et al., *JGR*, 2017

ULF Wave amplitude
$\mathbf{\Delta B} = \mathbf{B} - \mathbf{B}_0$
$\mathbf{B}_0$ sliding average

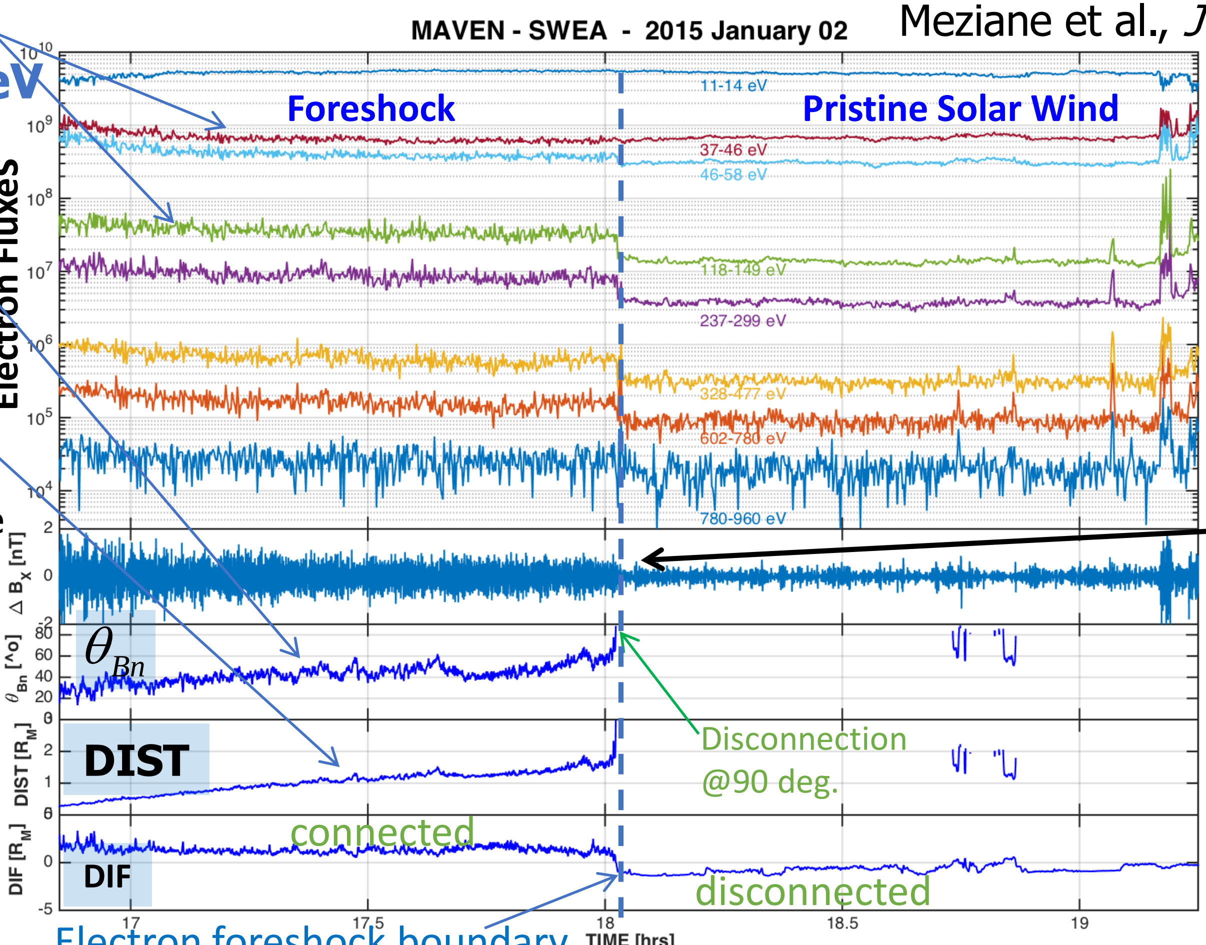

Electron foreshock boundary

(2)
Drop of the amplitude of pickup ions (protons) ULF waves in the pristine SW compared to the foreshock

Systematically observed **when crossing** the FSh boundary

Apparent discrepancy with the theory for the variation versus θ_{Bn} !... Why?

The distance along the magnetic field is more relevant for the flux decay.

Influence of the foreshock electrons on pickup proton induced waves?

Magnetic field fluctuations – Flux – Distance

Electrons

ULF Wave amplitude

$$\Delta \mathbf{B} = \mathbf{B} - \mathbf{B}_0$$

$\mathbf{B}_0$ sliding average

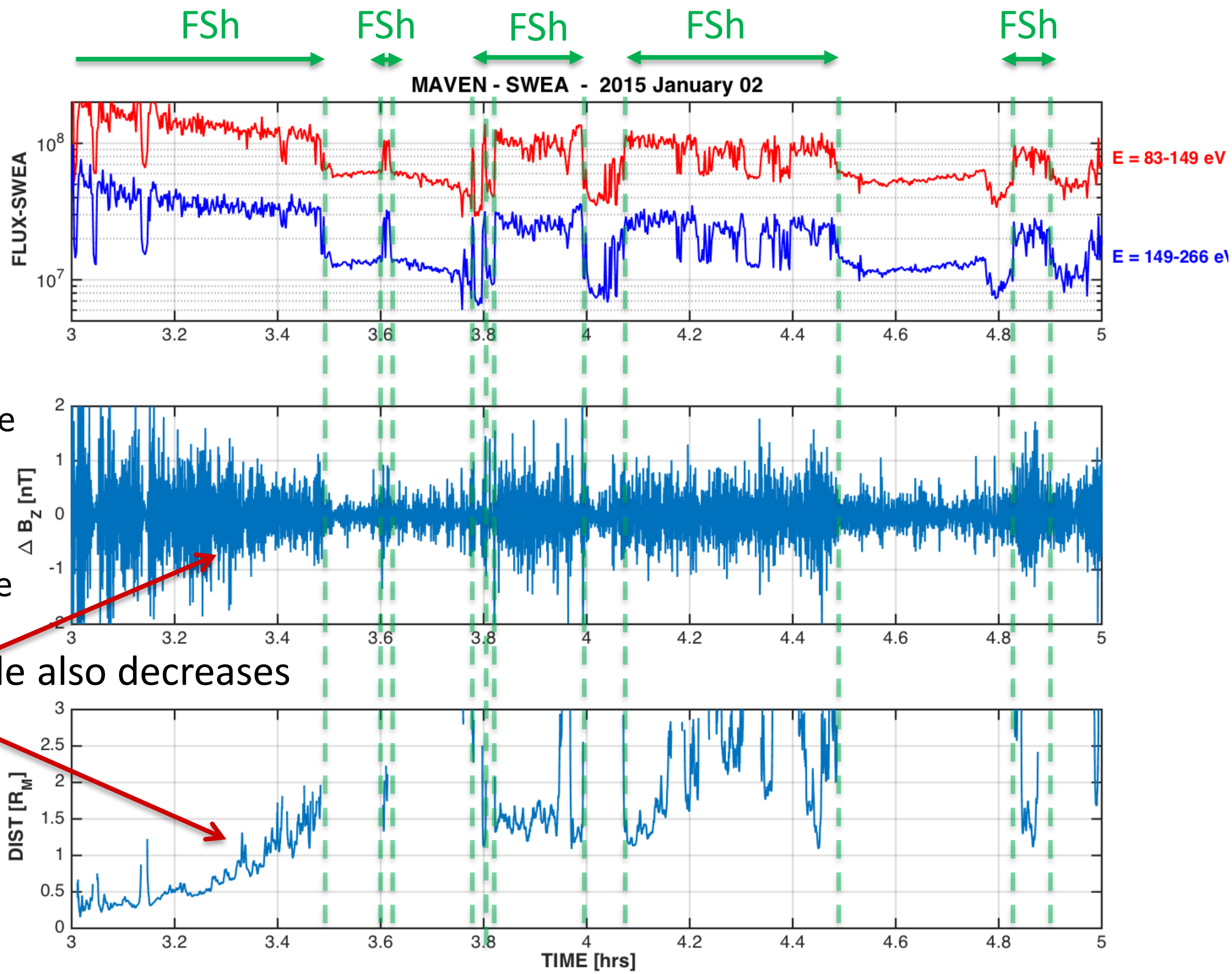

Wave amplitude also decreases with distance along B

Nearly one-to-one correspondance between electron foreshock boundary crossings and amplifications of the planetary pickup protons generated ULF waves.

other events

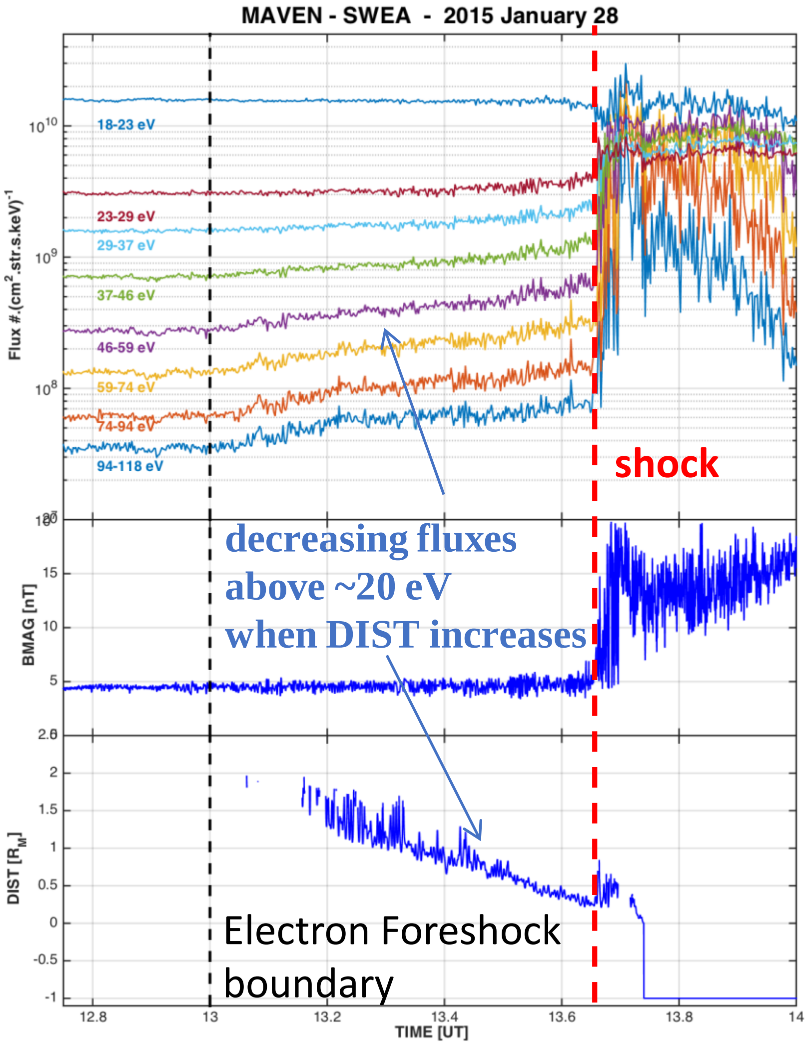

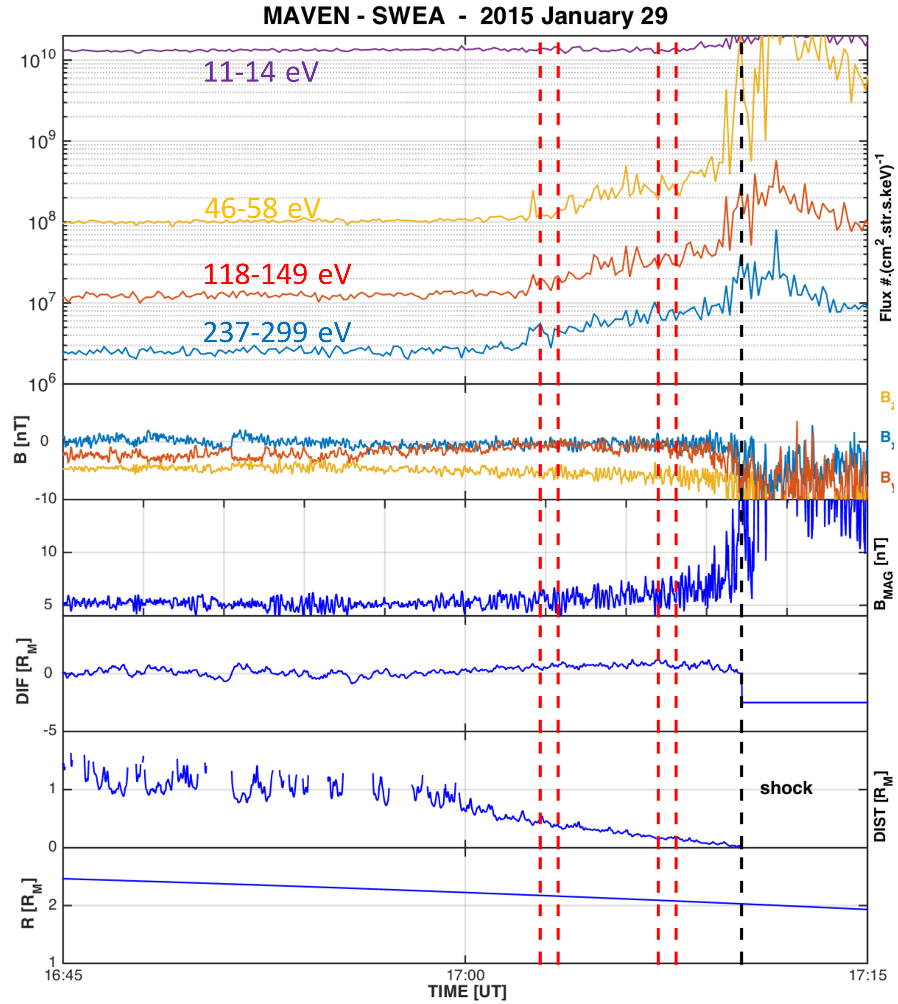

All cases identified up to now and fully analyzed are **always** showing the same feature.

Too small scale at Mars to expect an effect of electron microinstabilities (wave generation).

Martian exosphere

IUVS Observations of Atomic Components

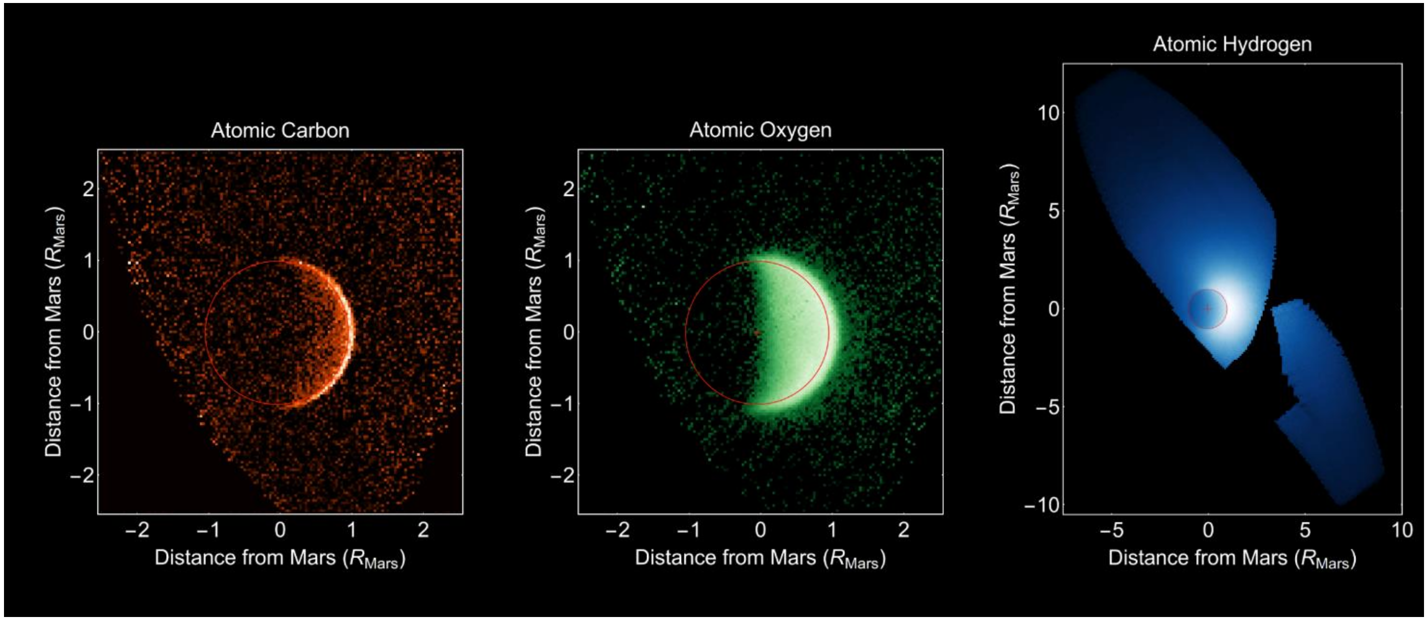

[Chaffin et al. 2015]

Mars has an extended exosphere **expanding far upstream the bow shock** (in particular for H): this is a **source of pickup ions which generate ULF waves** observed at frequencies nearly matching the local ion cyclotron frequencies as for comets [Wu & Davidson, 1972; Gary & Madland, 1988; Brinca, 1991].

Such 'proton cyclotron waves' have been reported at Mars [Russell *et al.*, 1990; Brain *et al.*, 2002; Bertucci, 2003; Mazelle *et al.*, 2004; Wei and Russell, 2006; Wei *et al.*, 2011; 2014; Connerney *et al.*, 2015; Romanelli *et al.*, 2012; 2016; 2018; Bertucci *et al.*, 2013; Ruhunusiri *et al.*, 2015] from Phobos-2, Mars Global Surveyor and MAVEN observations.

Pickup proton waves

An example of PCWs from MAVEN MAG data

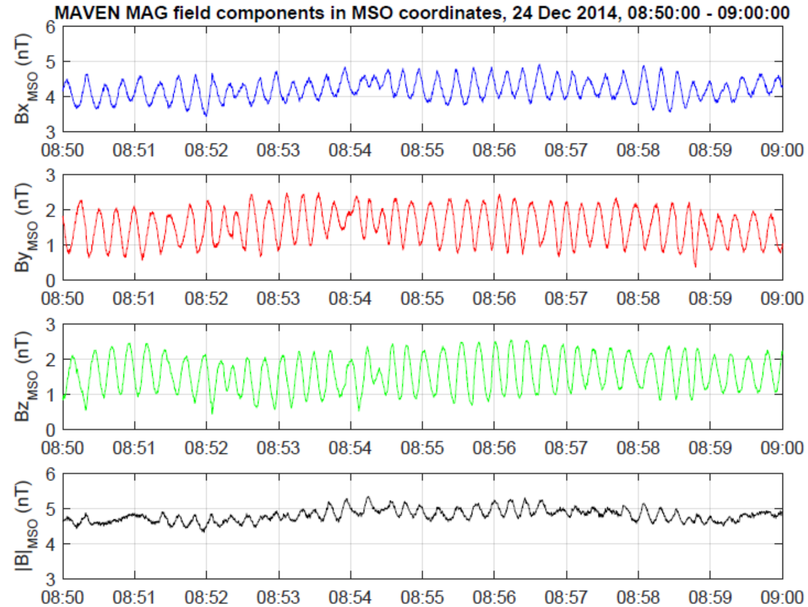

Romanelli, et al., JGR, 2017

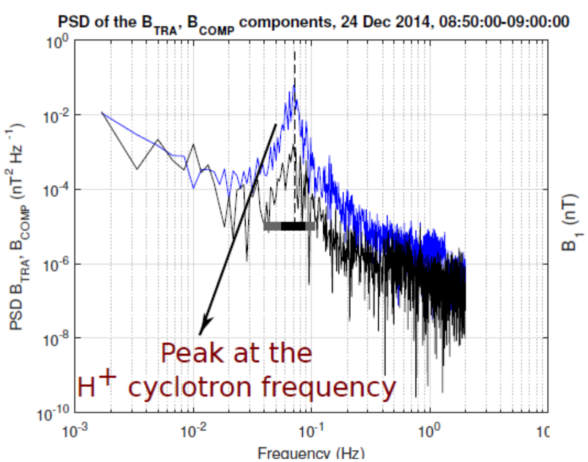

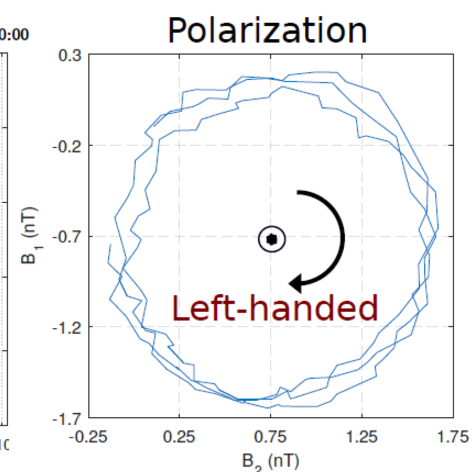

Wave amplitude amplification in the foreshock

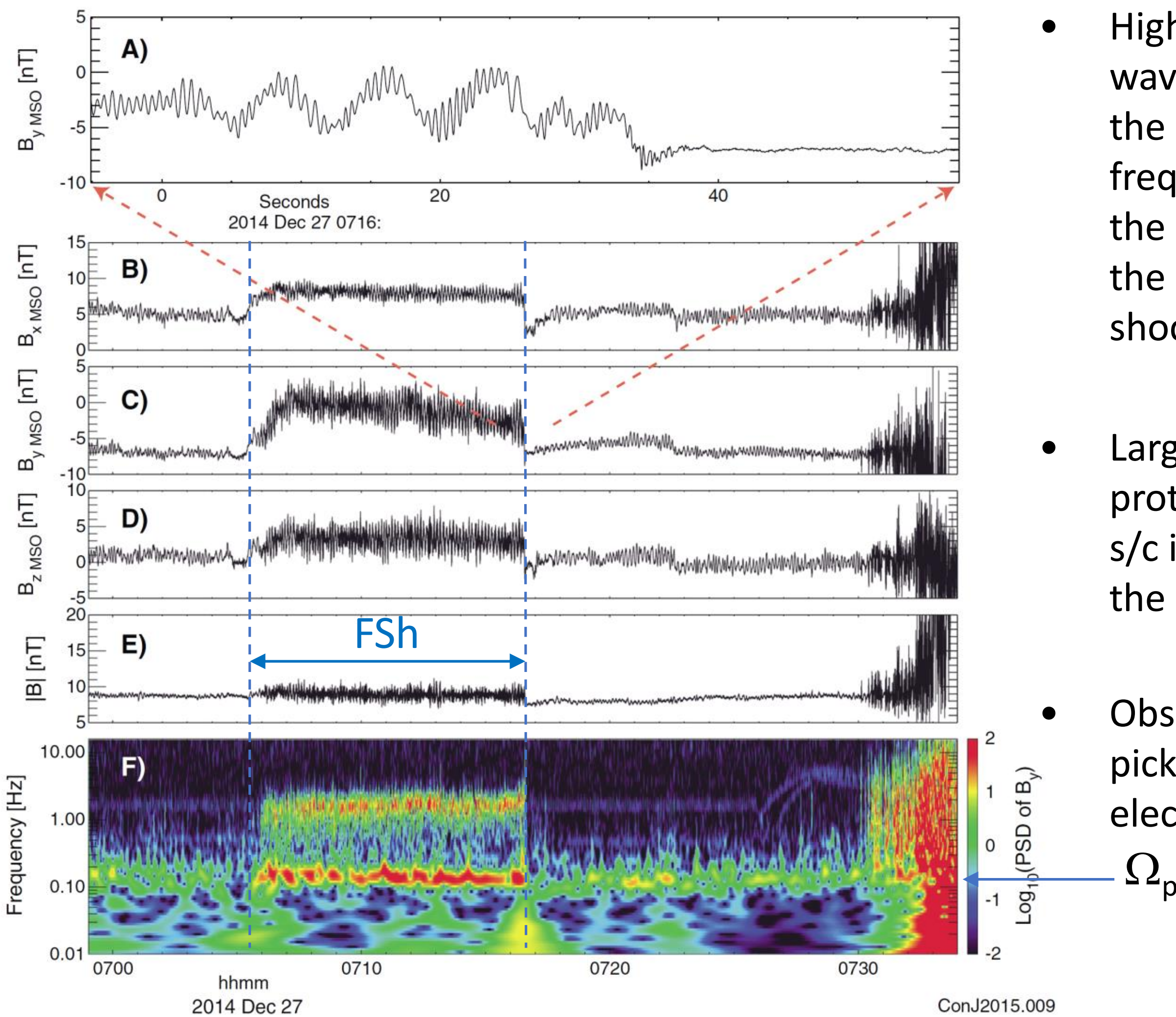

(After Connerney et al., GRL, 2015)

- Higher frequency waves (so called '1 Hz waves' at Earth) seen superimposed on the waves at the proton cyclotron frequency (pickup ions waves). At Earth the '1 Hz' waves are seen only inside the foreshock (most likely source at the shock).
- Larger ULF waves amplitude at the proton cyclotron frequency when the s/c intercepts a field-line connected to the bow shock (electron foreshock).
- Observation consistent with a higher pickup ion production rate inside the electron foreshock.

Wave amplitude amplification in the foreshock

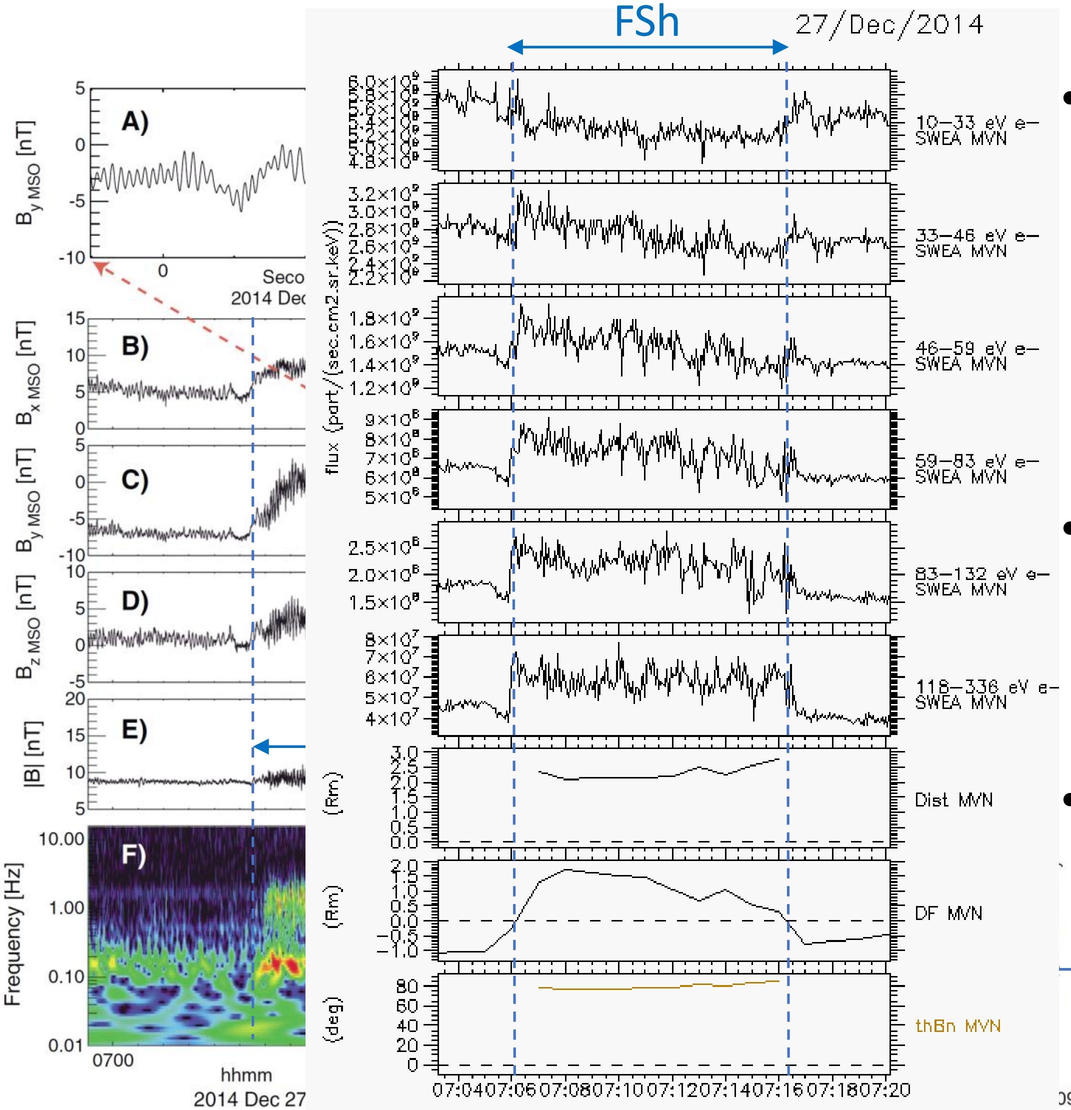

- Higher frequency waves (so called ‘1 Hz waves’ at Earth) seen superimposed on the waves at the proton cyclotron frequency (pickup ions waves). At Earth the ‘1 Hz’ waves are seen only inside the foreshock (most likely source at the shock).
- Larger ULF waves amplitude at the proton cyclotron frequency when the s/c intercepts a field-line connected to the bow shock (electron foreshock).
- Observation consistent with a higher pickup ion production rate inside the electron foreshock.

(After Connerney et al., GRL, 2015)

Electron Impact Ionization

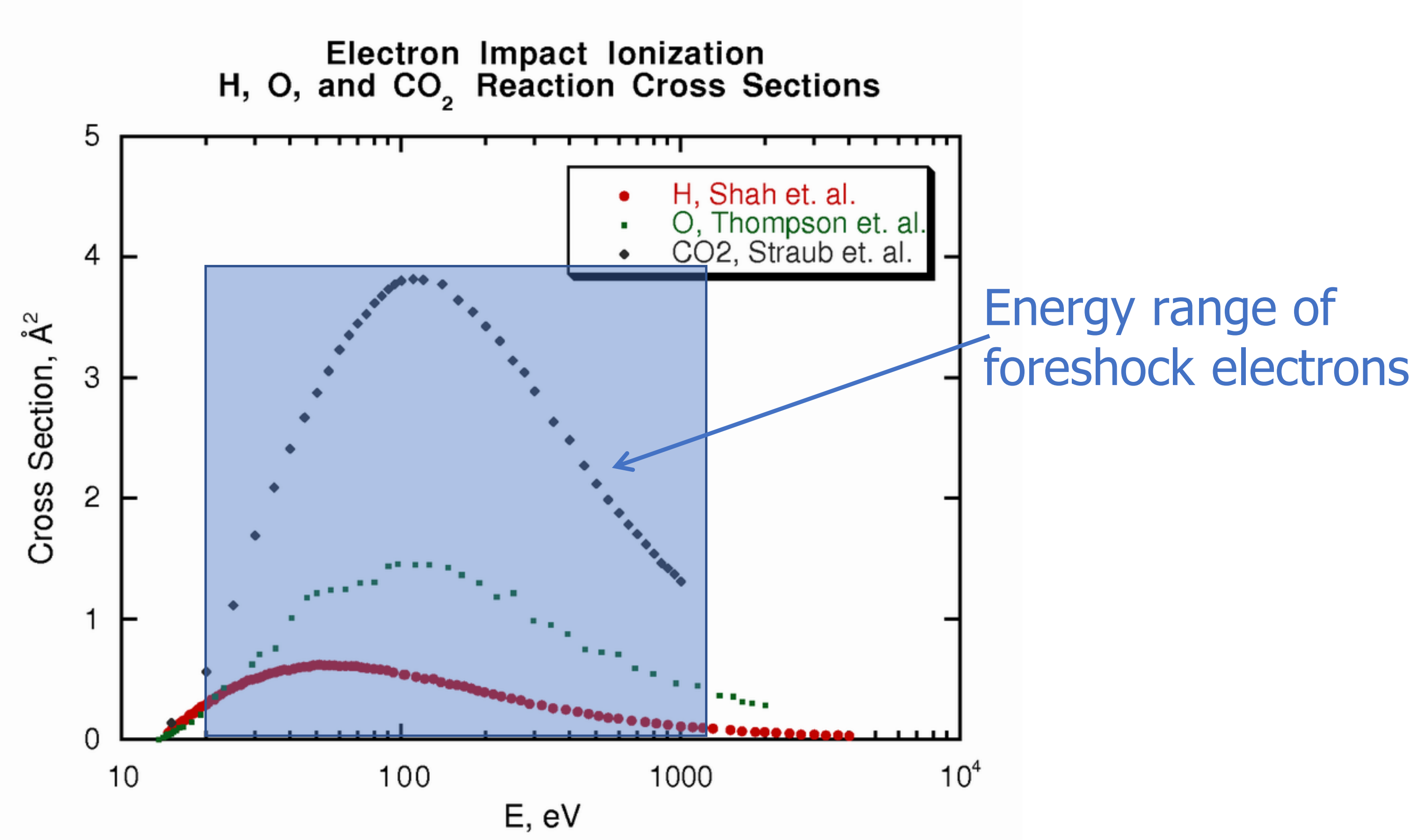

Higher wave amplitude is observed when more energetic electrons are present, so also higher pickup ion density (source of the waves). So this could be due to higher electron impact ionization rate (on H and O non thermal corona).

This needs to be quantified.

Foreshock Electron Impact Ionization (EII) (1)

- Let us assume that the flux decay with the distance is due to the impact with **exospheric atomic hydrogen** (as a first step).
- Consider a **monoenergetic electron beam** with energy E emanating from the shock and moving along the magnetic field.
- At a distance *x*, the flux is $\Gamma_E(x)$, where ***x*** **is the distance along the ambient magnetic field**.
- The variation of the flux is governed by the following equation:

$$\frac{d\Gamma_E(x)}{\Gamma_E(x)} = -n_H(x)\sigma(E)dx \qquad [1]$$

where $n_H(x)$ is the hydrogen density profile and $\sigma(E)$ is the EII cross-section

Integrating between $x = x_1$ and $x = x_2$

$$Ln\left(\frac{\Gamma_E(x_2)}{\Gamma_E(x_1)}\right) = -\sigma(E)\int_{x_1}^{x_2} n_H(x)dx = -\sigma(E)I(x_1, x_2) \qquad [2]$$

Foreshock Electron Impact Ionization (EII) (2)

- Let us first assume a simple power law profile for the **exospheric atomic hydrogen density** such as $n_H(x) = cx^{-\alpha}$, then it gives

$$Ln\left(\frac{\Gamma_E(x_2)}{\Gamma_E(x_1)}\right) = -\frac{c\sigma(E)}{1-\alpha}\left[x_2^{1-\alpha} - x_1^{1-\alpha}\right] \qquad [3]$$

- This can be tested for different energy ranges:

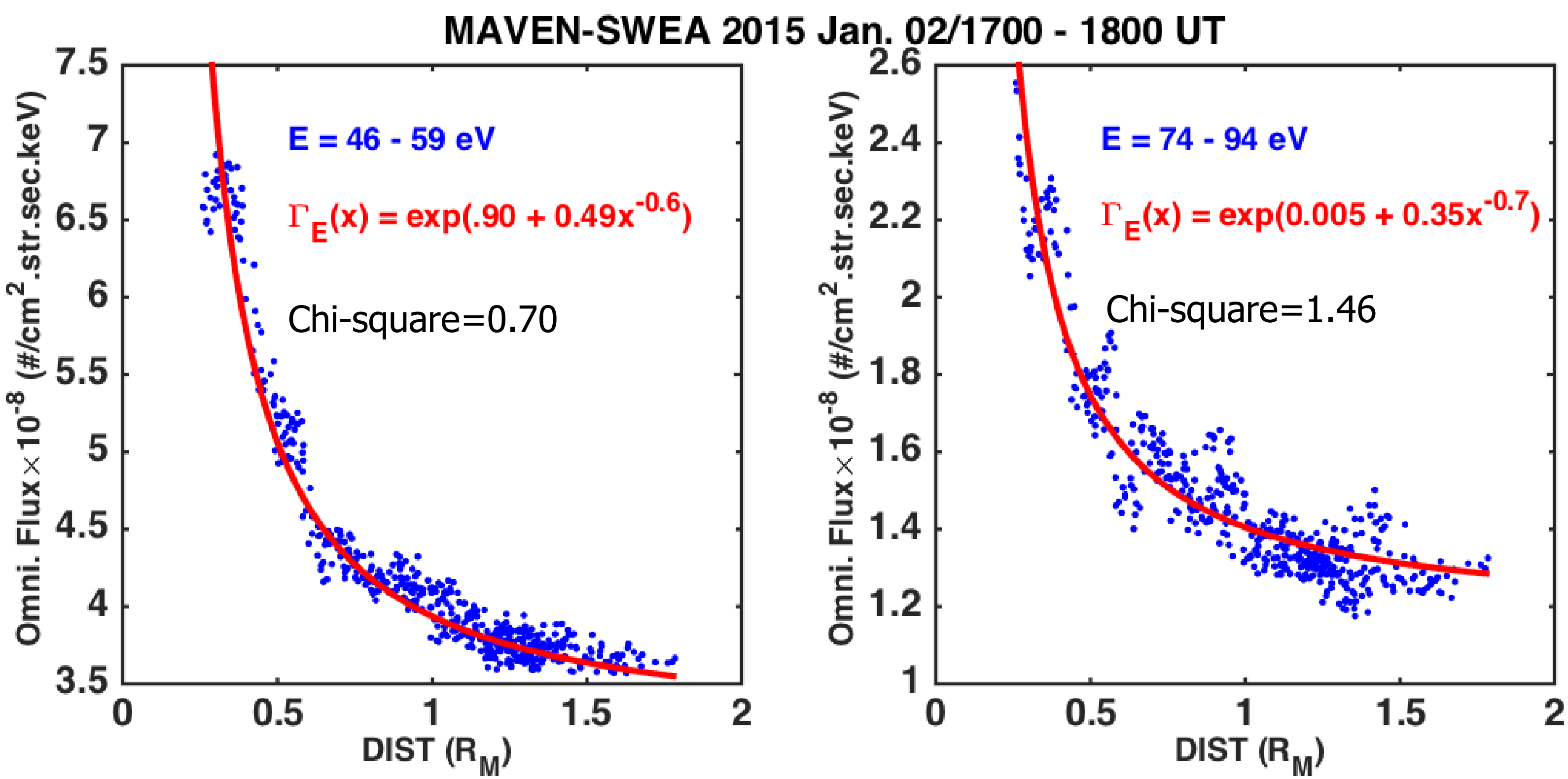

Good agreement: foreshock electrons fluxes attenuation due to EII with neutral H

Foreshock Electron Impact Ionization (EII) (3)

- Taking the same index as the one derived by Feldman et al. [2011] from Rosetta ALICE measurements: $n_H(r) \propto r^{-2.1}$ where r is the radial distance gives $\Gamma_E(x) \propto \exp(\, a + b \; x^{-1.1})$
- It should be a valid approximation only for large distances and B exactly radial so that $r \sim \mathrm{x}$ from the vectorial composition **r** = **ρ** + **x** , where **ρ** is the vector position of the connection point at the shock from the planet center.

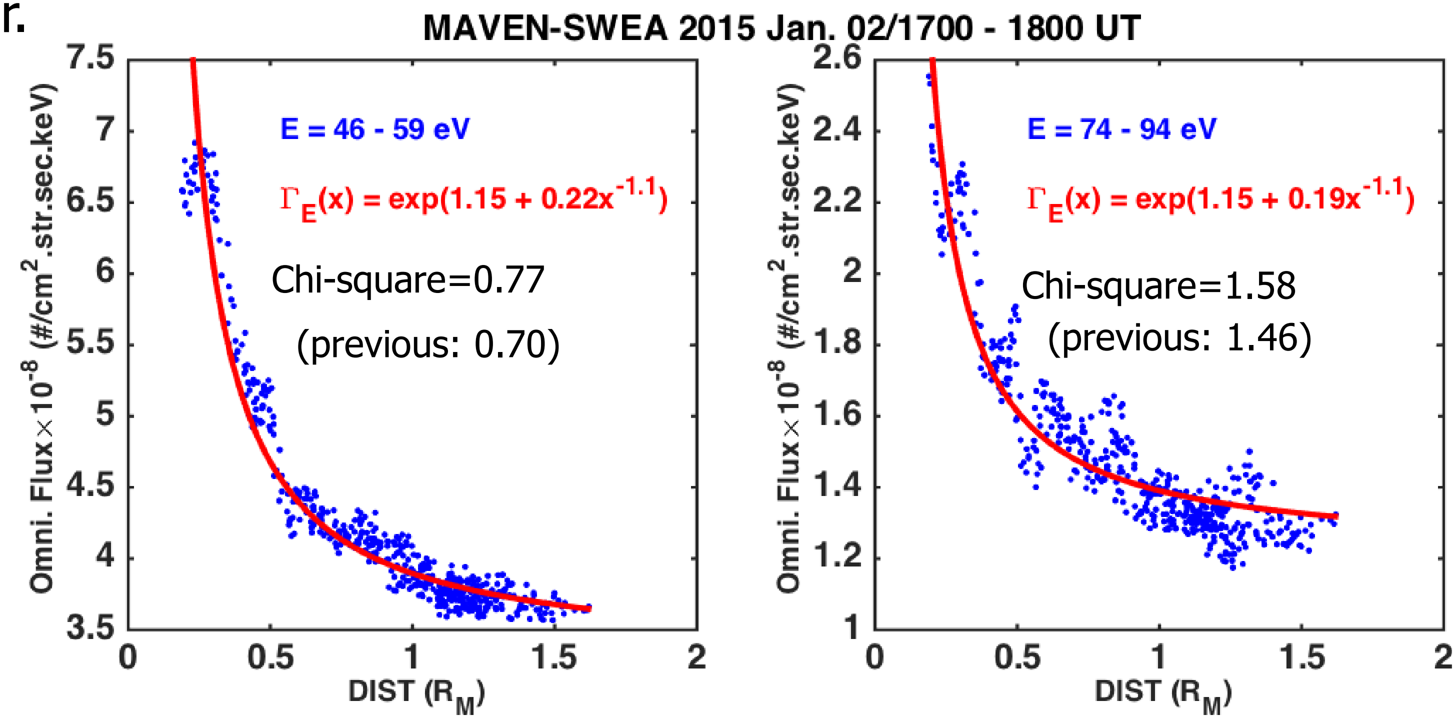

Little less good agreement but still consistent using the 1-D hydrogen radial profile

Foreshock Electron Impact Ionization (EII) (4)

Pursuing our analysis further and in order to precise the comparison with the model, both the distance and the **exospheric hydrogen density profile** are eliminated from the comparison.

Considering two arbitrary energy channels E_1 and E_2, let's build the ratio

$$\xi = \frac{\ln \frac{\Gamma_{E_1}(x_1)}{\Gamma_{E_1}(x_2)}}{\ln \frac{\Gamma_{E_2}(x_1)}{\Gamma_{E_2}(x_2)}} = \frac{\sigma(E_1)}{\sigma(E_2)}$$

from the electron fluxes for two instants t_1 and t_2 sufficiently distant and corresponding to two spacecraft positions x_1 and x_2

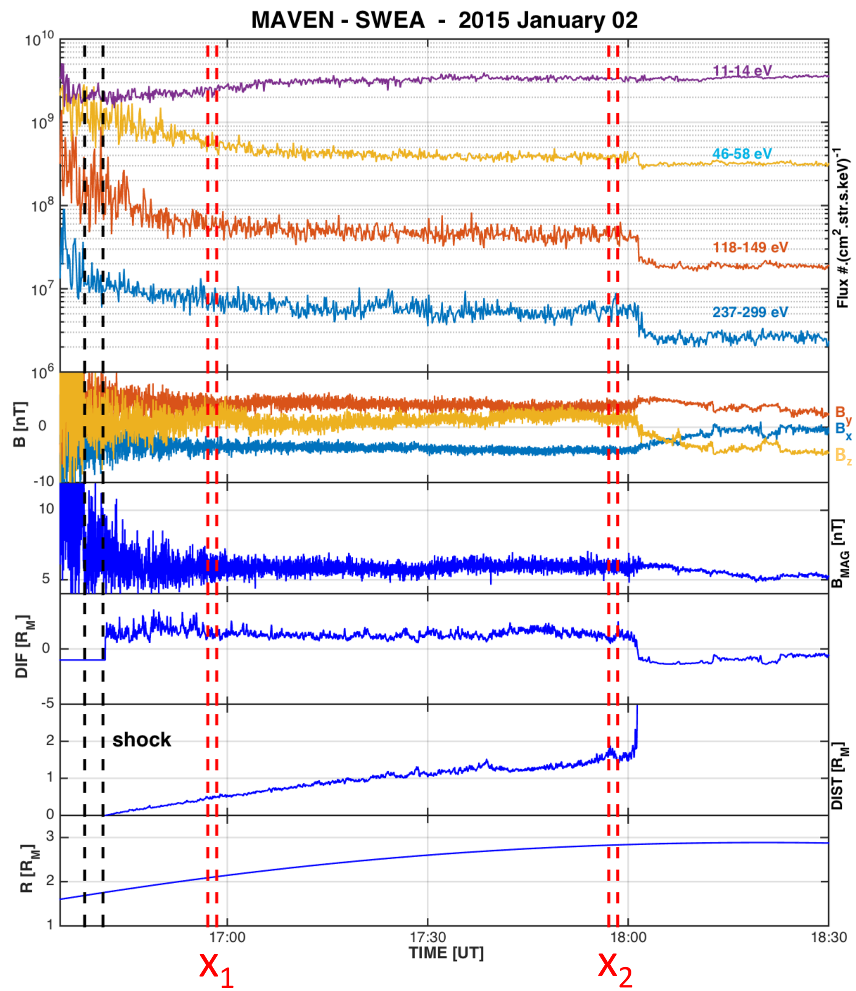

Comparison with different profiles of EII cross-sections

The variation of $\xi_{E_0}(E)$ for E_0 = 52.1 eV (black closed circles) for two events are compared with the electron-Atomic hydrogen cross sections ratio $\left(\frac{\sigma(E)}{\sigma(E_0)}\right)$ from different available cross-sections in the literature.

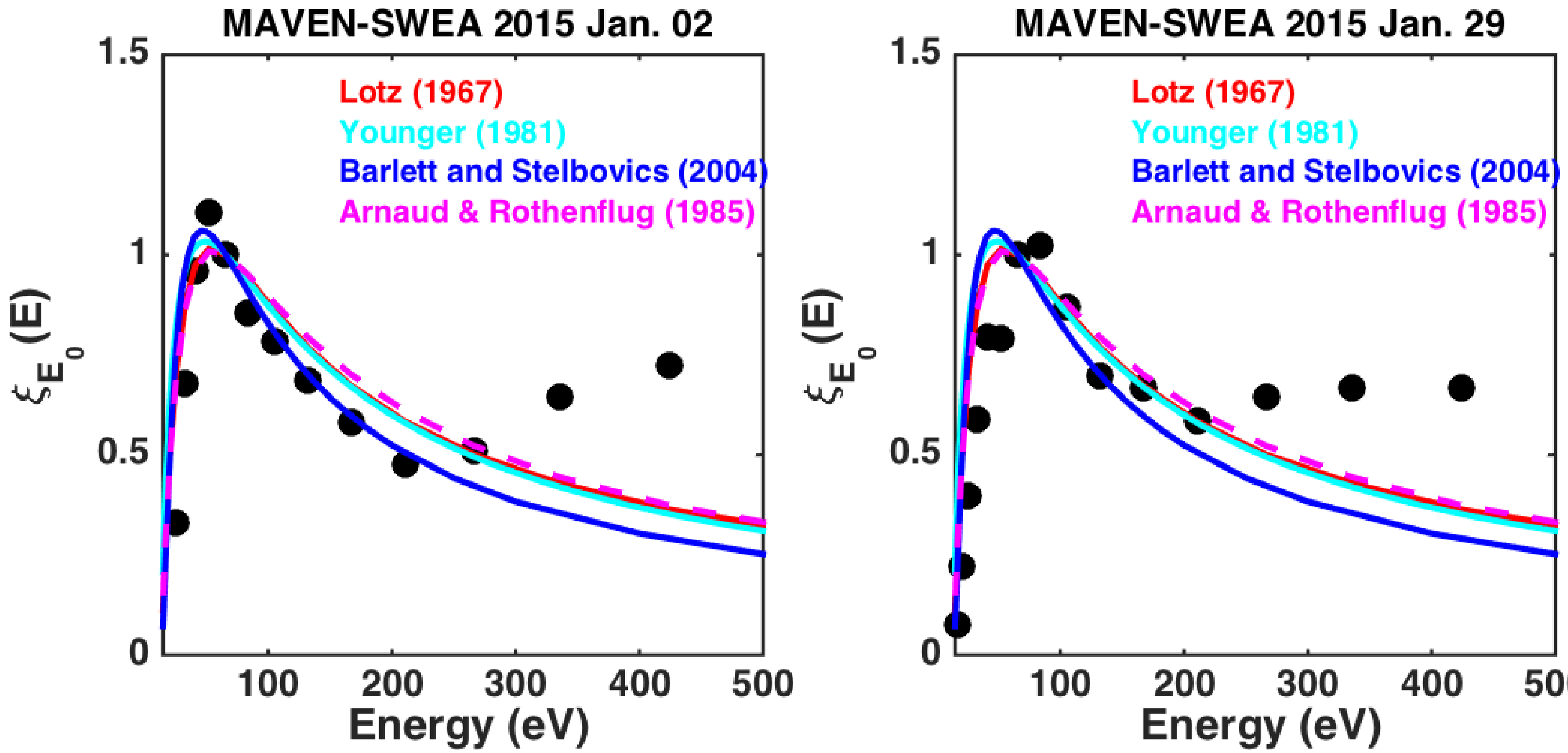

As predicted by the present model, the empirical cross section tracks well the observed flux ratio for electron energy E ≤ 250 eV (lack of impact on oxygen? Other reason?)

Mazelle *et al.*, *Geophys. Res. Lett.*, 2018

Conclusion: Martian Electron Foreshock

- Apparent discrepany with the terrestrial 'paradigm' for the backtreaming electrons produced by Fast Fermi acceleration.
- Flux fall-off of the foreshock electrons is well reproduced by a simple 1-D analytical model describing the effect of **impact ionization on neutral exospheric hydrogen atoms.**
- This is the **first evidence** of this process upstream from the bow shock of Mars where it is usually neglected in the models.
- A complete calculation could be made using a more realistic 3-D model of the neutral hydrogen density.
- Conversely, the foreshock electron fluxes fall-off could be used **to put constraint on the local hydrogen density profile at high altitudes.** For every MAVEN orbit crossing the bow shock, a large part of the upstream path is inside the electron foreshock.
- **New complementary tool to constraint hydrogen exosphere.**
- It plays a role by increasing the production of **pickup protons** (and subsequent 'proton cyclotron waves') which are both related to atmospheric escape.

Mazelle *et al.*, *Geophys. Res. Lett.*, 2018

CU/LASP • GSFC • UCB/SSL • LM • JPL

MAVEN Detects Steep Drop in Hydrogen Escape at Mars

MAVEN has detected an unexpectedly precipitous drop in the hydrogen escape rate from Mars over the course of a Mars year. Independent observations from four MAVEN instruments show a factor of 10 decrease in the abundance of hydrogen in the corona, corresponding to a similar decrease in the neutral H escape rate. The decline in coronal density occurs as Mars goes from perihelion to aphelion. There is no definitive explanation as to why the decrease should be more than a factor of two.

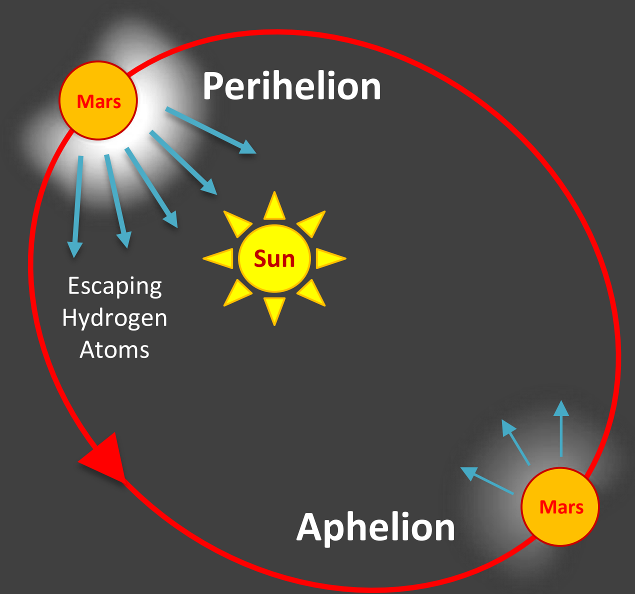

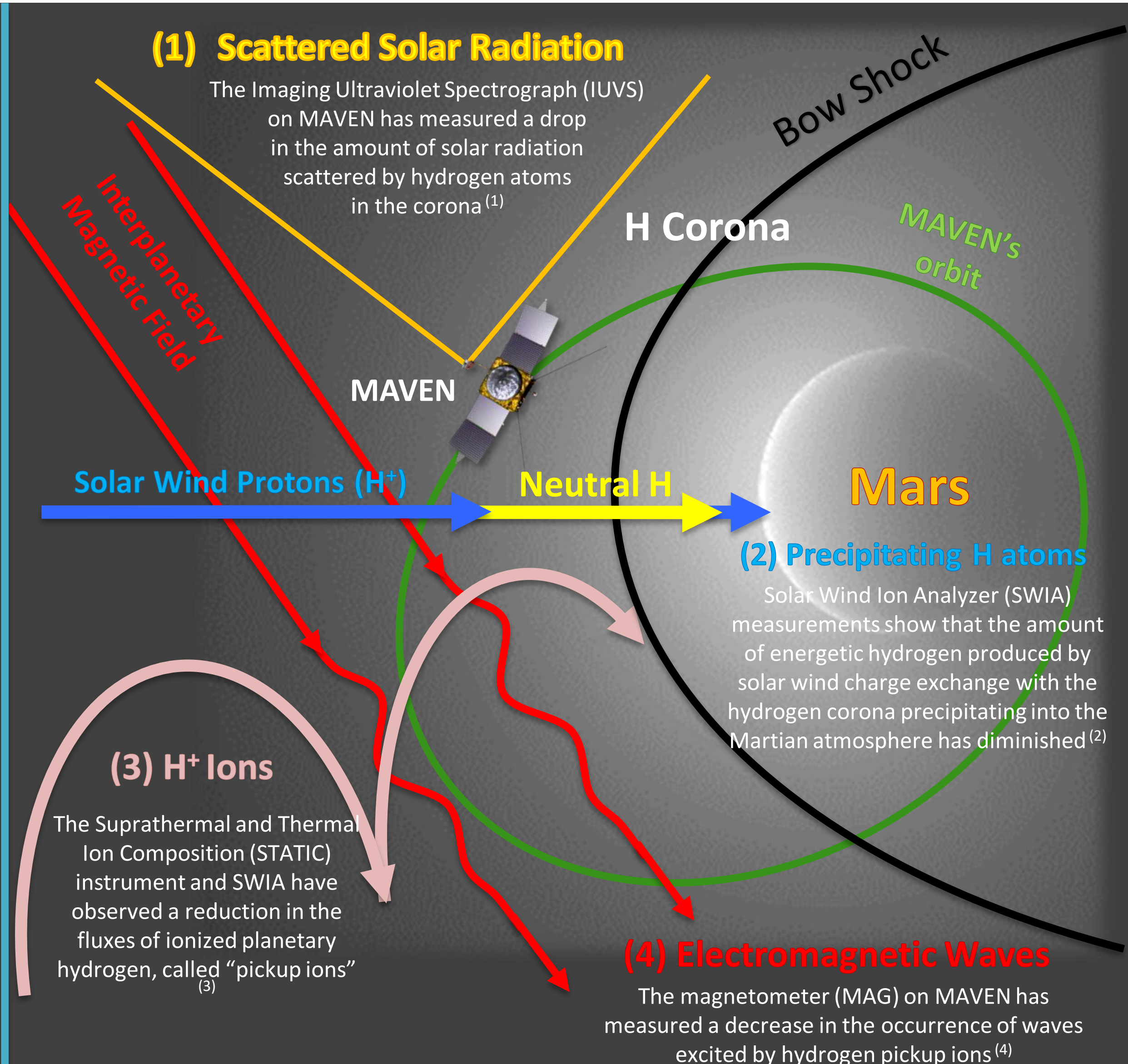

(1) Clarke et al. (2) Halekas et al. (3) Rahmati et al. (4) Romanelli et al. (JGR MAVEN Special Issue, 2016)